UNIVERSITY OF
FLORIDA

Department of Materials Science and Engineering

Ph: (352) 392-6664
FAX: (352) 392-4911
E-mail: pholl@silica.mse.ufl. edu

258 A Rhines Hall
PO Box 116400
Gainesville, FL 32611-6400
(352) 392-6664
Fax: (352) 392-4911

October 15, 1996

Dr. Y.S. Park
Office of Naval Research
800 North Quincy Street
Arlington, VA 22217-5000

Dr. Anis Husain
Defense Sciences Office
DARPA
3701 N. Fairfax Drive
Arlington, VA 22203-1714

Dear Drs. Park and Husain,

Attached is a progress report summarizing activities in our URI entitled "Blue Light Emitting Materials and Injection Devices" under grant number N00014-92-J-1895. The period summarized is from June 1, 1996 to August 31, 1996.

Sincerely,

Paul

Paul H. Holloway
Professor

xc: Dr. A. Goodman
Dr. Tom Walker
Dr. Diego Olego

f:urioct96.doc

DISCLAIMER NOTICE

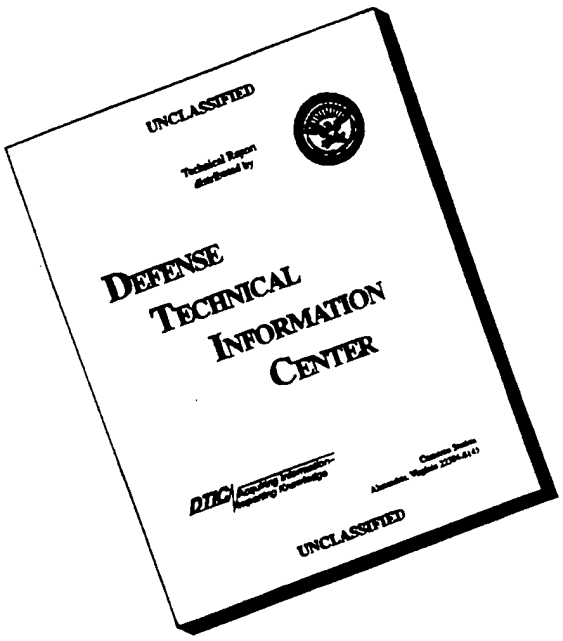

THIS DOCUMENT IS BEST QUALITY AVAILABLE. THE COPY FURNISHED TO DTIC CONTAINED A SIGNIFICANT NUMBER OF PAGES WHICH DO NOT REPRODUCE LEGIBLY.

REPORT DOCUMENTATION PAGE

FORM APPROVED
OMB No. 0704-0188

1. AGENCY USE ONLY (Leave blank)	2. REPORT DATE	3. REPORT TYPE AND DATES COVERED
	Oct. 15, 1996	Quarterly - Jun. 1, 1996 to Aug. 31, 1996

4. TITLE AND SUBTITLE OF REPORT

Visible Light Emitting Materials and Injection Devices

5. FUNDING NUMBERS

ONR Grant
N00014-92-J-1895

6. AUTHOR(S)

Paul H. Holloway

7. PERFORMING ORGANIZATION NAME(S) AND ADDRESS(ES)

Department of Materials Science and ENgineering
University of Florida
P.O. Box 116400
Gainesville, FL 32611-6400

8. PERFORMING ORGANIZATION REPORT NUMBER:

N/A

9. SPONSORING/MONITORING AGENCY NAME(S) AND ADDRESS(ES)

Office of Naval Research
800 North Quincy Street
Arlington, VA 22217-5000

10. SPONSORING/MONITORING AGENCY REPORT NUMBER:

11. SUPPLEMENTARY NOTES:

12a. DISTRIBUTION AVAILABILITY STATEMENT

Unlimited

12b. DISTRIBUTION CODE

13. ABSTRACT (Maximum 200 words)

Progress in report on research into ZnSe-based and GaN-based materials and devices for light emitting diodes and diode lasers at blue-green visible wavelengths.

14. SUBJECT TERMS

Zinc Selenide
Gallium Nitride
Light Emitting Diodes
Diode Lasers

15. NUMBER OF PAGES: 53

16. PRICE CODE

17. SECURITY CLASSIFICATION OF REPORT:	18. SECURITY CLASSIFICATION OF THIS PAGE	19. SECURITY CLASSIFICATION OF ABSTRACT	20. LIMITATION OF ABSTRACT
None	None	None	None

Quarterly Progress Report

June 1, 1996 to August 31, 1996

Visible Light Emitting Materials and Injection Devices

ONR/DARPA URI

Grant Number N00014-92-J-1895

Prepared by:

Paul H. Holloway
Department of Materials Science and Engineering
University of Florida
P.O. Box 116400
Gainesville, FL 32611
Ph: 352/392-6664; FAX: 352/392-4911
E-Mail: Internet - pholl@silica.mse.ufl.edu

Participants:
University of Florida
Kevin Jones
Robert Park
Joseph Simmons
Cammy Abernathy
Stephen Pearton
Dept. Materials Science and Engineering
Timothy Anderson
Dept. of Chemical Engineering
Peter Zory
Dept. of Electrical Engineering
Columbia University
Gertrude Neumark
Dept. of Materials Science and Engineering
Oregon Graduate Institute of Science and Engineering
Reinhart Engelmann
Dept. of Electrical Engineering

(I) Growth by MBE and Characterization of GaN (Robert Park)

III-V Nitride Work

During this quarter, our MBE GaN work focused on a novel growth method which we call "alternate element exposure" (AEE) in which the group III and group V elements do not impinge on the surface at the same time. The basic concept of GaN growth by AEE is the promotion of Ga adatom migration on growing surfaces under N-free conditions which can be achieved, we have discovered, at temperatures much lower than those required for conventional MBE growth. In this work the growth temperature using the AEE technique was 600°C. By virtue of forming a Ga-covered surface at relatively low temperatures and, hence, a chemically active surface, the sticking coefficient of N can be enhanced.

The RHEED specular beam intensity was recorded during Ga and N shutter operating sequences and a typical behavior is shown in Fig. I.1 for the case of a 30 sec. delay time. In each cycle, the N shutter was opened. The Ga exposure time was 5 seconds. After the Ga shutter was closed, a 30 second delay was introduced in this case before the N shutter was again opened. The delay time was varied systematically from run to run, example times being 0 sec., 15 sec., 30 sec., and 50 sec. A total of 2000 shutter cycles were performed for the growth of each AEE sample.

Conventional MBE-grown GaN films were deposited on c-plane sapphire substrates at a growth temperature around 700°C. Attempts to grow GaN films conventionally at lower temperatures resulted in Ga droplet formation over the growing surface since the Ga atom diffusion rate is slow compared to the growth rate of the GaN film. In general, all of our conventionally grown films, regardless of the growth temperature, exhibited PL spectra having a broadband, yellow emission at ~2.3 eV. This yellow band luminescence is thought to be associated with native, deep-level defect transitions which suppress the more desirable UV luminescence. A low temperature PL spectrum recorded from a 0.3μm thick conventionally grown GaN film is shown in Fig. I.2. The growth temperature was 600°C.

On the other hand, samples grown using the AEE technique did not exhibit the yellow band emission in their PL spectra. Fig. I.3 shows the low temperature PL spectra recorded from GaN films grown using various Ga-delay times, namely 0 sec., 15 sec., 30 sec., and 50 sec. As can be seen from the figure, the yellow-band emission is absent from all of the spectra. It also appears from this data that there is an optimum Ga-delay time (in this case 30 sec.) which produces the most efficient near band-edge emission. Work is in progress which is aimed at understanding this phenomenon.

(II) Growth and processing of GaN-based materials (Cammy Abernathy and Steve Pearton)

II.a Contacts - Comparison Of Ohmic Metallization Schemes for InGaAlN

While significant advances in the processing of III-V nitrides has resulted in nitride-based blue/UV light emitting and electronic devices, problems still exist. One major area of concern is ohmic contacts. It has proven difficult to produce low resistance ohmic contacts to the III-nitride materials because of their wide bandgaps. Many metallization schemes have been

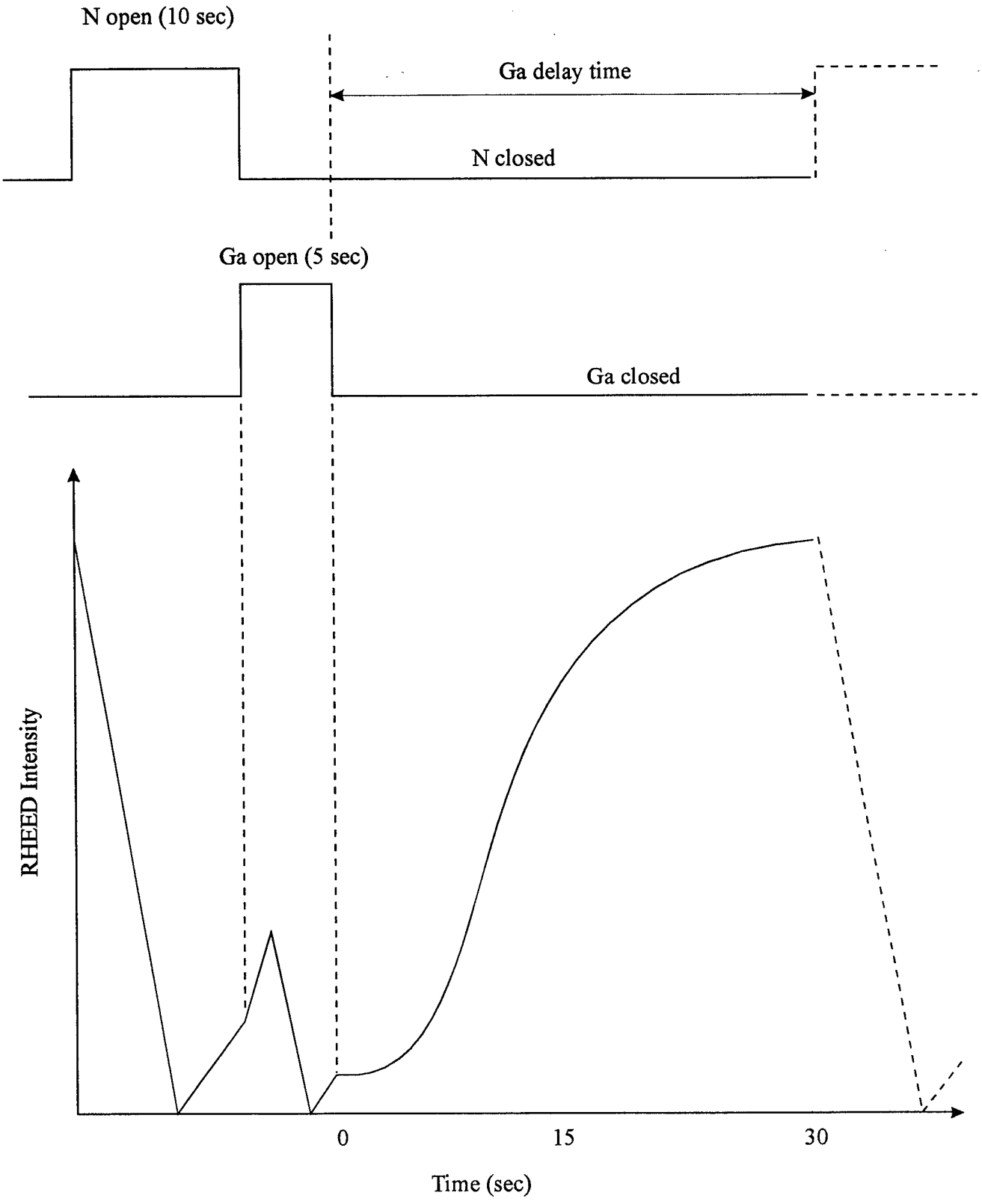

Fig. I.1. RHEED specular beam intensity as a function of time during Ga and N shuttering.

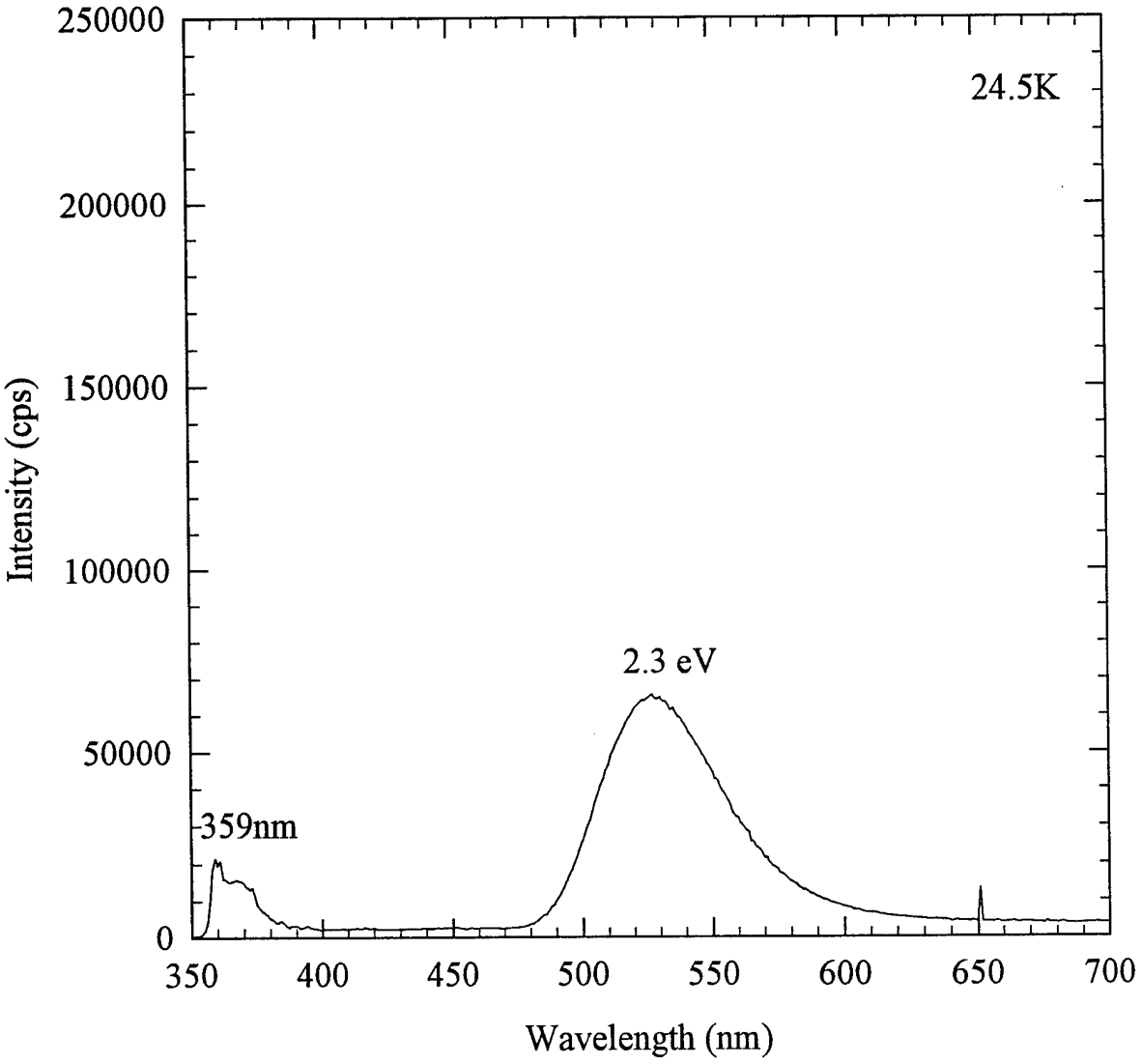

Fig. I.2. PL spectrum recorded from a GaN film grown by conventional MBE growth at 600°C (Film thickness = 0.3 μm)

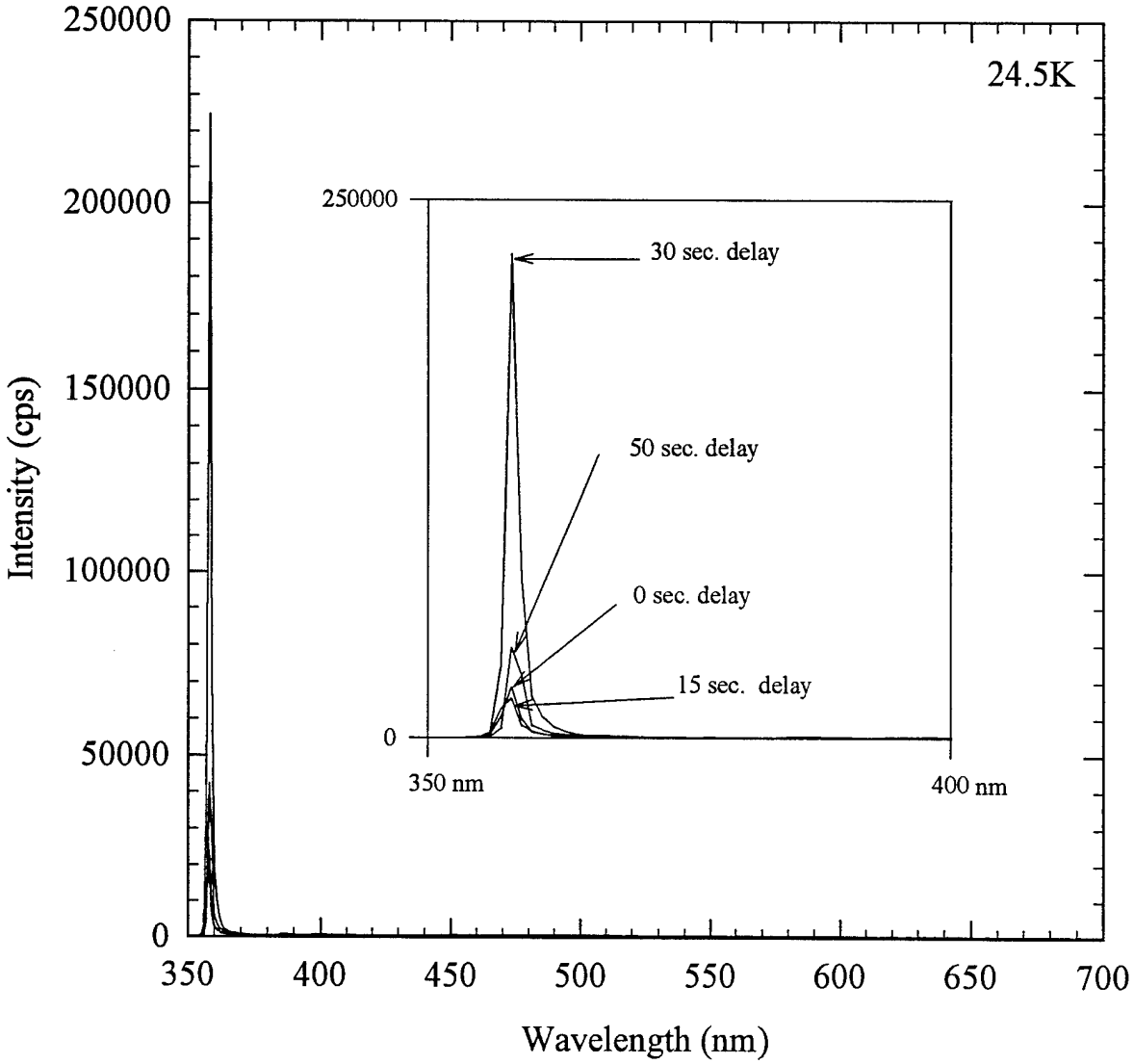

Fig. I.3. PL spectra recorded from GaN films grown by the AEE technique using various Ga-delay times, namely, 0 sec., 15 sec., 30 sec., and 50 sec.

tried, including Au and Al single metal contacts to n^+ GaN and non- alloyed Au/Ti and Al/Ti, which were found to have contact resistances of ~ 10^{-3} to 10^{-4} $\Omega \cdot cm^2$. The lowest contact resistance reported for n^+ GaN was a Ti/Al contact annealed at 900°C for 30 sec in a rapid thermal annealer ($\rho_c = 8x10^{-6}$ $\Omega \cdot cm^2$). The authors suggested the formation of a TiN interface as important in the formation of the low resistance contact. Ohmic contacts ($\rho_c \sim 10^{-4}$ $\Omega \cdot cm^2$) were produced with W to n^+ GaN with little interaction between the semiconductor and the metal up to 800°C. [13] WSi_x on n^+ GaN was found to be stable to 800°C as well, with a contact resistance of ~10^{-5} $\Omega \cdot cm^2$. Non-alloyed Ti/Pt/Au contacts to the lower bandgap material InN produced ohmic contacts with specific contact resistance $\rho_c = 1.8x10^{-7}$ $\Omega \cdot cm^2$. Graded contact layers to GaN have been formed with both InN and InGaN epilayers metallized with WSi_x. Graded $In_xGa_{1-x}As$/InN contacts have also been used on GaAs/AlGaAs heterojunction bipolar transistors, with ρ_c as low as $5x10^{-7}$ $\Omega \cdot cm^2$. A review of ohmic contact work to date has been published by Smith and Davis.

Reliability of contacts is also an issue, especially for high temperature electronics applications. The use of refractory metal contacts such as W and WSi_x may be a solution. Moreover, the contact resistance could be reduced if lower bandgap In-containing alloys (or InN) were used as contact layers on GaN, much as the case with InGaAs on GaAs. However, the In-based nitrides are less thermally stable than GaN, and we need to establish the trade off between better contact resistance and poorer temperature stability.

In this paper we report the results of experiments in which W, $WSi_{0.44}$ and Ti/Al contacts were deposited on n^+ $In_{0.65}Ga_{0.35}N$, n^+ InN and n^- $In_{0.75}Al_{0.25}N$. Graded InAlN contact layers were also examined. The electrical, structural and chemical stability of these contacts were investigated after anneals up to 900°C , using Transmission Line Method (TLM) measurements, Scanning Electron Microscopy (SEM) and Auger Electron Spectroscopy (AES). In addition, temperature dependent TLM measurements in the range 25°C to 125°C were taken for the non-graded samples- to obtain information about the conduction mechanism.

The 2000Å thick InGaN, InN and InAlN samples were grown using Metal Organic Molecular Beam Epitaxy (MO-MBE) on semi-insulating, (100) GaAs substrates in an Intevac Gen II system as described previously. The InN, $In_{0.65}Ga_{0.35}N$ and $In_{0.75}Al_{0.25}N$ were highly auto-doped n-type (~10^{20} cm^{-3}, ~ 10^{19} cm^{-3} and $8x10^{18}$ cm^{-3} respectively) due to the presence of native defects. The $In_xAl_{1-x}N$ ($x = 0.6 \rightarrow 1$) graded layers were grown on $In_{0.6}Al_{0.4}N$, auto-doped n-type (~10^{18} cm^{-3}).

The samples were rinsed in H_2O:NH_4OH (20:1) for 1 min just prior to deposition of the metal to remove native oxides. The metal contacts were sputter deposited to a thickness of 1000Å in the case of W and $WSi_{0.44}$, and then etched in SF_6/Ar in a Plasma Therm reactive ion etcher (RIE) to create TLM patterns. For the Ti/Al contacts, 200Å of Ti and then 1000Å of Al was deposited, and the TLM pattern formed by lift-off. The nitride samples were subsequently etched in $Cl_2/CH_4/H_2/Ar$ in an Electron Cyclotron Resonance (ECR) etcher to produce the mesas for the TLM patterns. The samples were annealed at temperatures from 300 to 900°C for 15 sec under a nitrogen ambient in a RTA system (AG-410).

The specific contact resistance for W, WSi_x and Ti/Al ohmic contacts to InGaN as a function of annealing temperature is shown in Fig. II.a.1. All contacts had similar contact resistance as deposited, ~ $2\text{-}4x10^{-7}$ $\Omega \cdot cm^2$. Above 600°C, the Ti/Al contacts degraded rapidly, and the WSi_x continued to degrade, while ρ_c for both samples increased up to ~ 10^{-5} $\Omega \cdot cm^2$ at

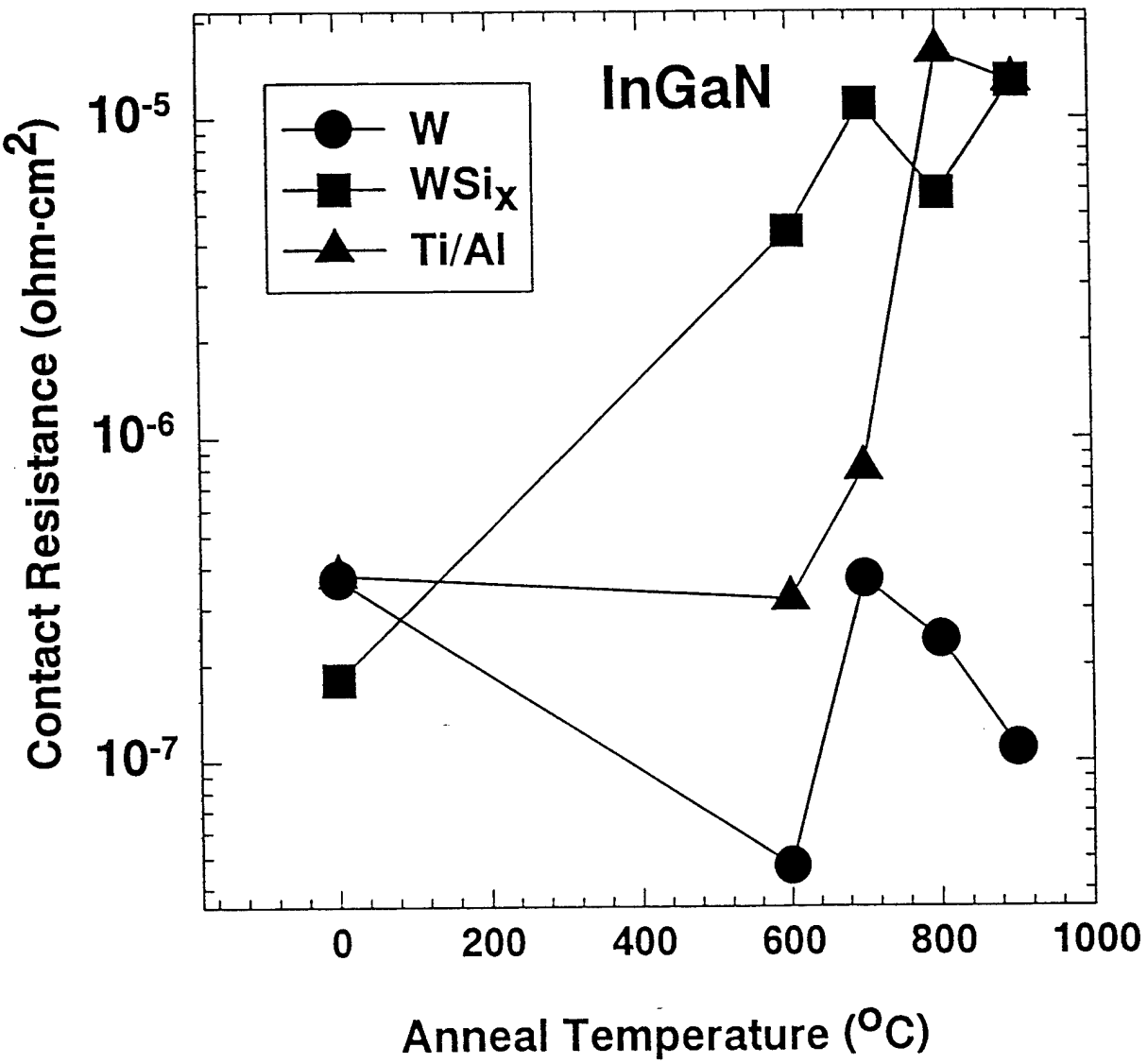

Fig. II.a.1.

Specific contact resistance for W, WSi_x or Ti/Al contacts on InGaN as a function of annealing temperature.

900°C. The error in these measurements was estimated to be ±10 % due mainly to geometrical contact size effects. The widths of the TLM pattern spacings varied slightly due to processing, (maximum of ± 5 %) as determined by SEM measurements, which were taken into account when calculating the contact resistances.

The specific contact resistance for ohmic contacts of W, WSi_x and Ti/Al to InN as a function of annealing temperature is shown in Fig. II.a.2 As-deposited samples had similar contact resistances to InGaN, indicating a similar conduction mechanism. WSi_x contacts showed the most degradation at low temperature, with the resistance rising a factor of 5 after 300°C annealing and then remaining constant. Ti/Al deviated little from initial values, although there was severe pitting on samples annealed at 500°C, while W resistance began to degrade at 500°C.

In Fig. II.a.3 the contact resistance is shown for W, WSi_x and Ti/Al ohmic contacts to InAlN as a function of annealing temperature. As-deposited Ti/Al had the lowest contact resistance on this material, $\rho_c \sim 1x10^{-4}\ \Omega \cdot cm^2$. W had the highest initial contact resistance, ($\rho_c \sim 1x10^{-2}\ \Omega \cdot cm^2$). The contacts showed morphological stability to 400°C (Ti/Al) to 800°C (W).

SEM micrographs of InAlN contacted with W, WSi_x and Ti/Al as grown and annealed at 800, 700 and 400°C respectively are shown in Fig. II.a.4 The W on InAlN remained smooth until 800°C, and then began to form hillocks, as did the WSi_x contact at 700°C. The Ti/Al began pitting above 400°C. The pitting in the Ti/Al contacts was due to diffusion of the Al through the Ti into the sample, as determined by AES depth profiles. Hillocks appear to be formed from diffusion of In from the nitride sample into the contact layer.

Fig. II.a.5 shows the specific contact resistance of WSi_x contacts directly on $In_{0.6}Al_{0.4}N$ (top) and InN graded from $In_{0.6}Al_{0.4}N$ (bottom) as a function of anneal temperatures up to 700°C. The values for the non-graded contacts are $\sim 5x10^{-4}\ \Omega \cdot cm^2$ and are stable to 700°C. The graded contacts show a drop in specific contact resistance at 500 °C to $\sim 1x10^{-5}\ \Omega \cdot cm^2$. AES depth profiles of WSi_x/InN/graded $In_xAl_{1-x}N$/InAlN as grown Fig. II.a.6 (top) and after 500 °C anneal (bottom) show little change in near surface composition. N has diffused out into the WSi_x and may have formed an interfacial WN_2 phase which plays a role in the lower contact resistance.

Fig. II.a.7 shows the theoretical curves for contacts to InGaN of this doping level exhibiting thermionic, thermionic field, or field emission as their dominant conduction mechanisms. The curves are shown only to give the expected temperature dependence of ρ_c and the magnitude of the specific contact resistance is arbitrary. The theoretical values are calculated from

$\rho_c \alpha \exp(\Phi_b/E_{00})$ for field emission

$\rho_c \alpha \exp[\Phi_b/E_{00}\coth(qE_{00}/kT)]$ for thermionic field emission

$\rho_c \alpha \exp(q\Phi_b/kT)$ for thermionic emission

where

$E_{00} = h/4\pi[N_d/m^*\varepsilon_s]^{1/2}$

with Φ_b being the barrier height, N_d the donor concentration in the semiconductor, m* the effective mass of electrons in the material and ε_s the permittivity of the semiconductor. For field emission $qE_{00}/kT >> 1$, for thermionic field emission $qE_{00}/kT \sim 1$, and for thermionic emission $qE_{00}/kT << 1$, with $q/kT \cong 0.026$ eV at 300 K. A fixed barrier height (1 eV) was assumed for calculations of the three conduction mechanisms. As values have not been definitively

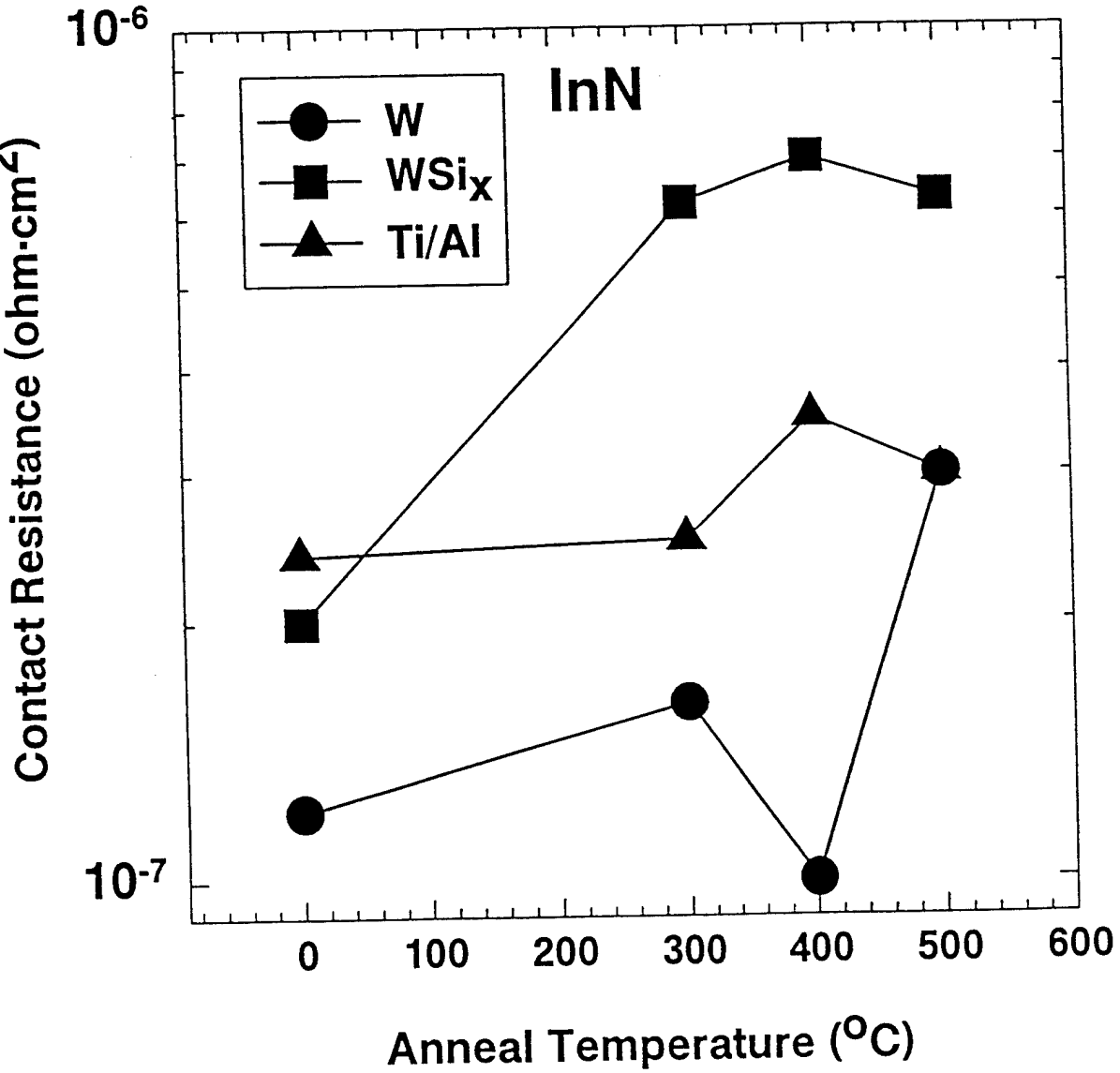

Fig. II.a.2.

Specific contact resistance for W, WSi_x or Ti/Al contacts on InN as a function of annealing temperature.

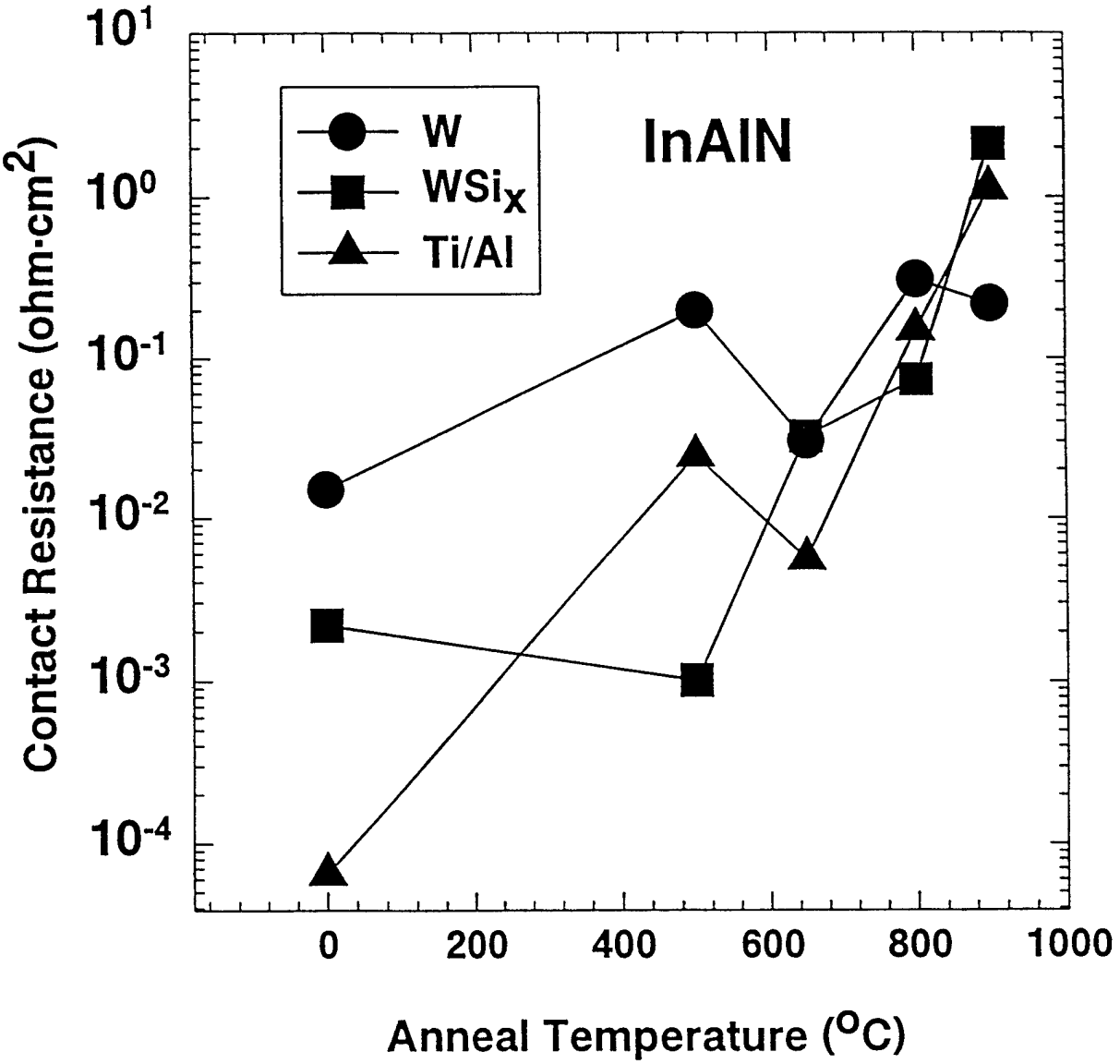

Fig. II.a.3.

Specific contact resistance for W, WSi_x and Ti/Al ohmic contacts to InAlN as a function of annealing temperature.

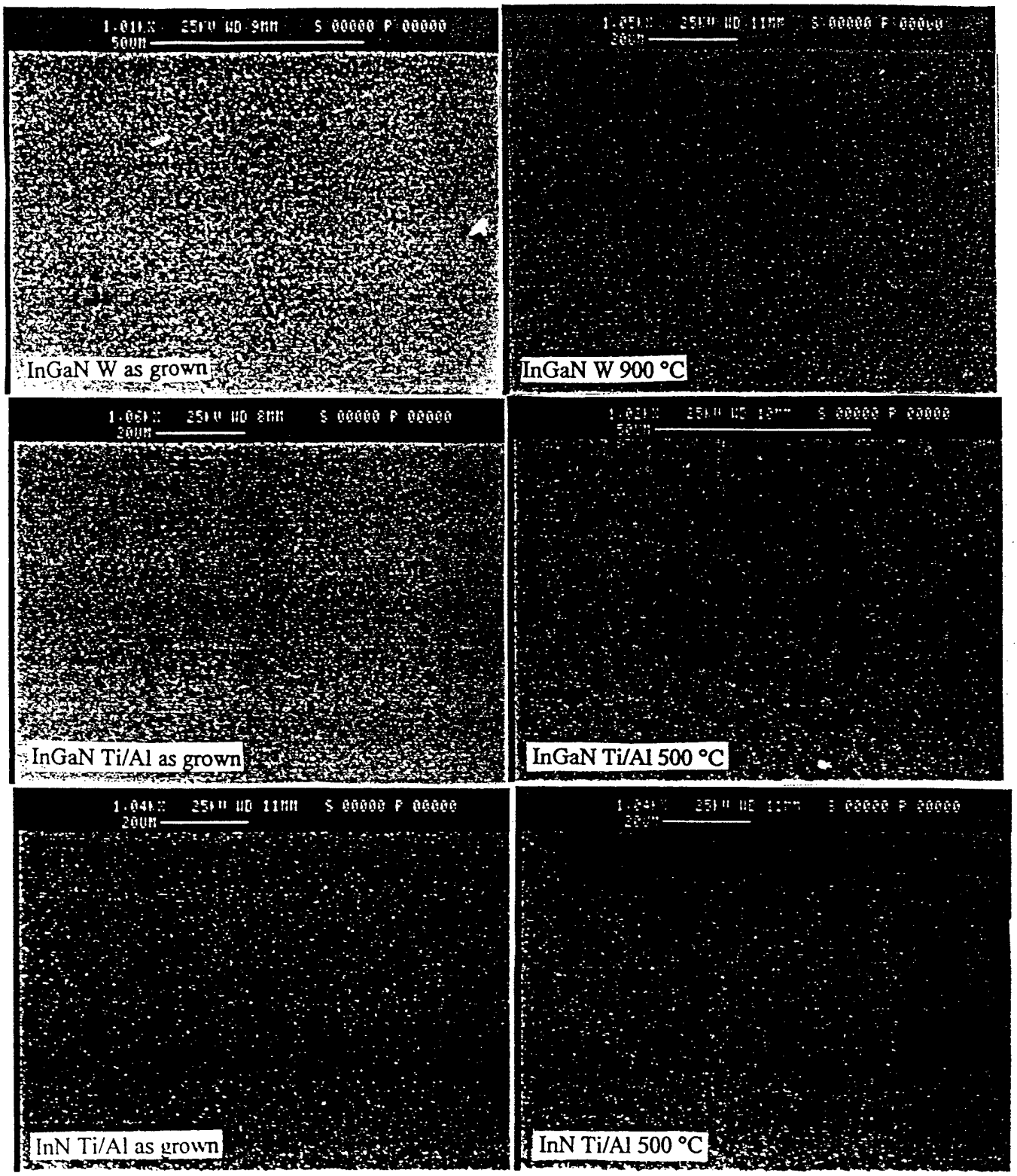

Fig. II.a.4.

SEM micrographs of W contacts on InGaN as-grown (top right) and annealed at 900 °C (top left), Ti/Al contacts on InGaN as-grown (bottom left) and annealed at 500 °C (bottom right).

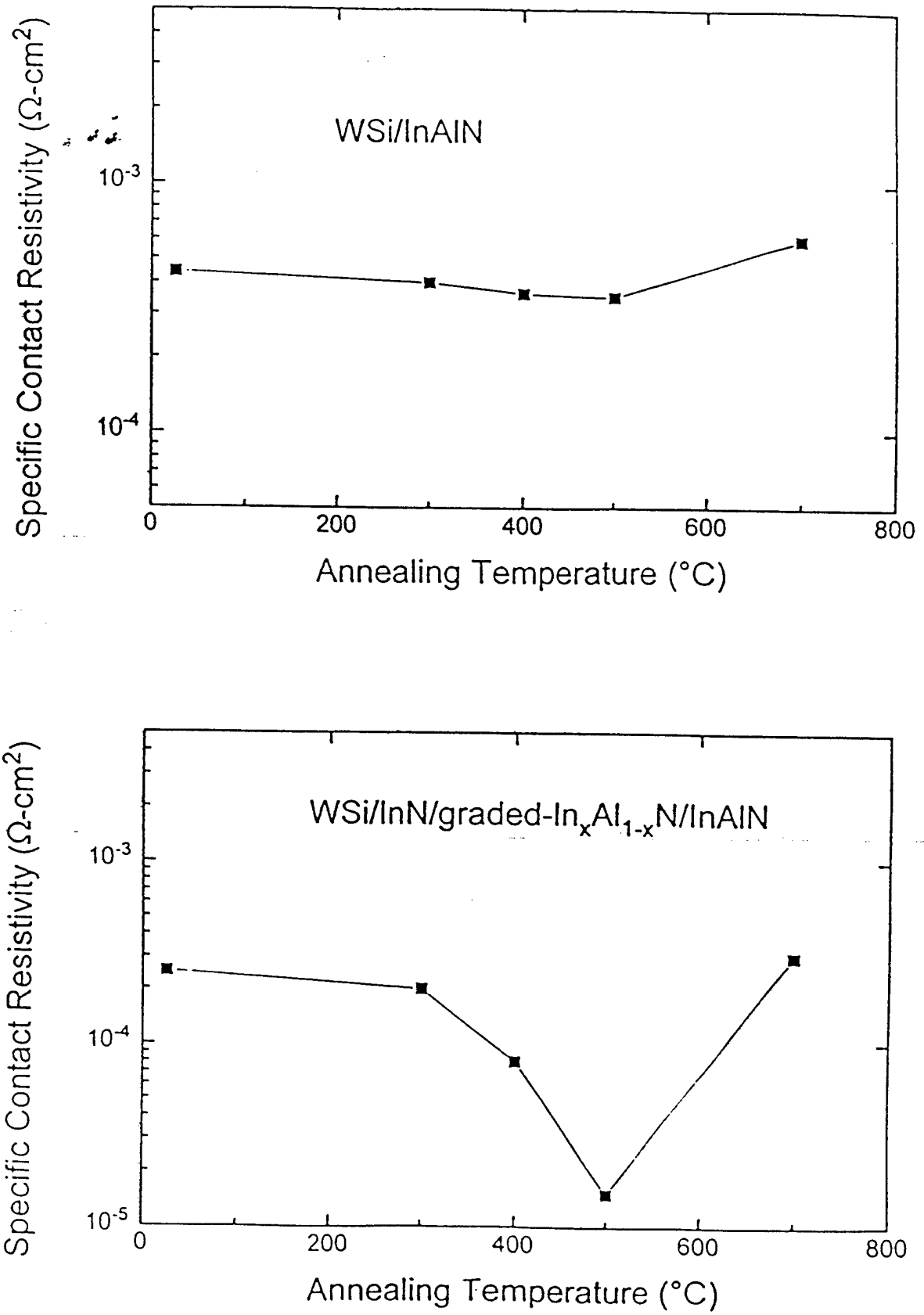

Fig. II.a.5. Specific contact resistance of WSi_x contacts to $In_{0.6}Al_{0.4}N$ (top) and InN graded to $In_{0.6}Al_{0.4}N$ (bottom) as a function of anneal temperature.

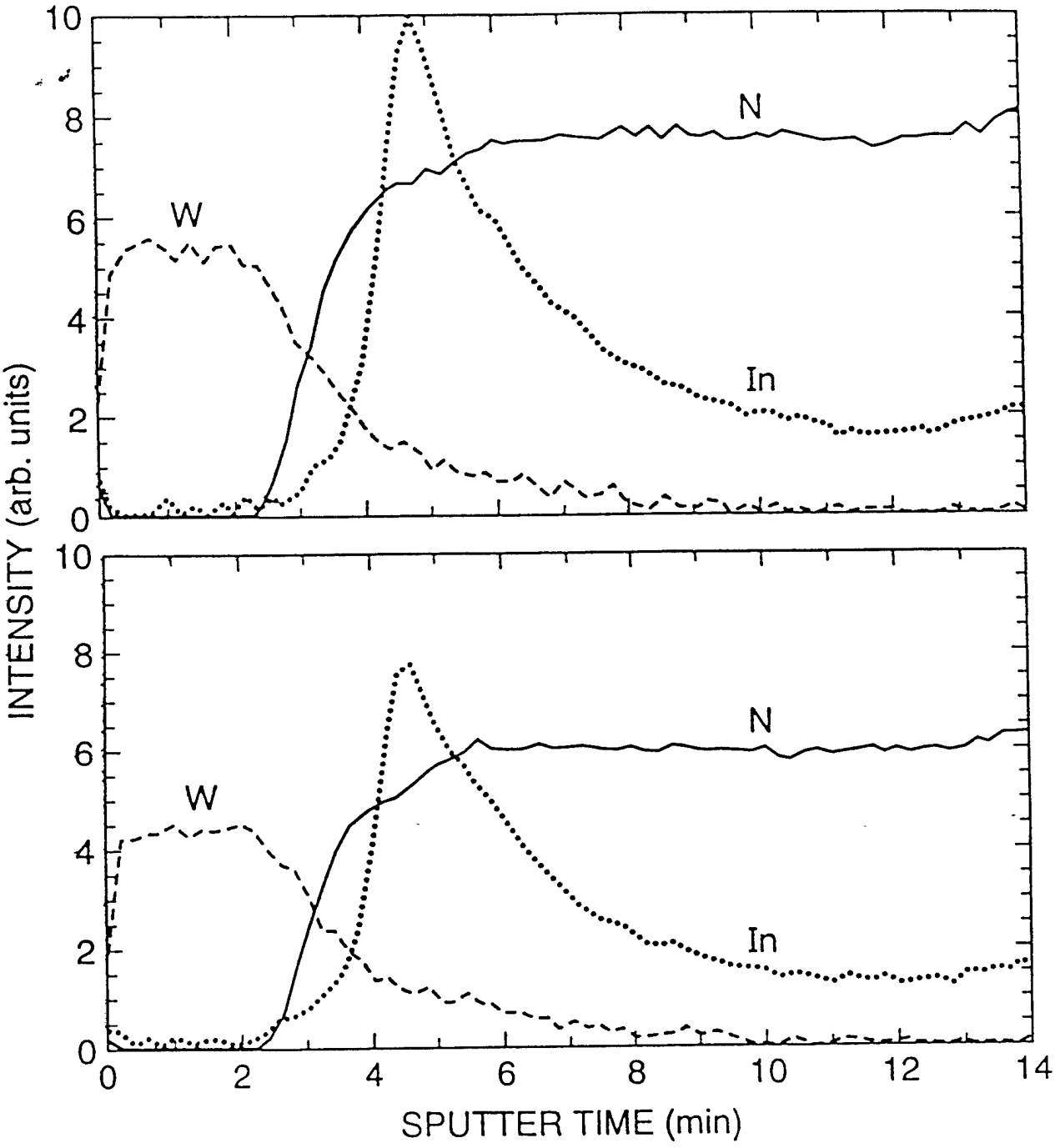

Fig. II.a.6.

AES depth profiles of W/InN/graded $In_xAl_{1-x}N$/InAlN as grown (top) and after 500 °C anneal (bottom).

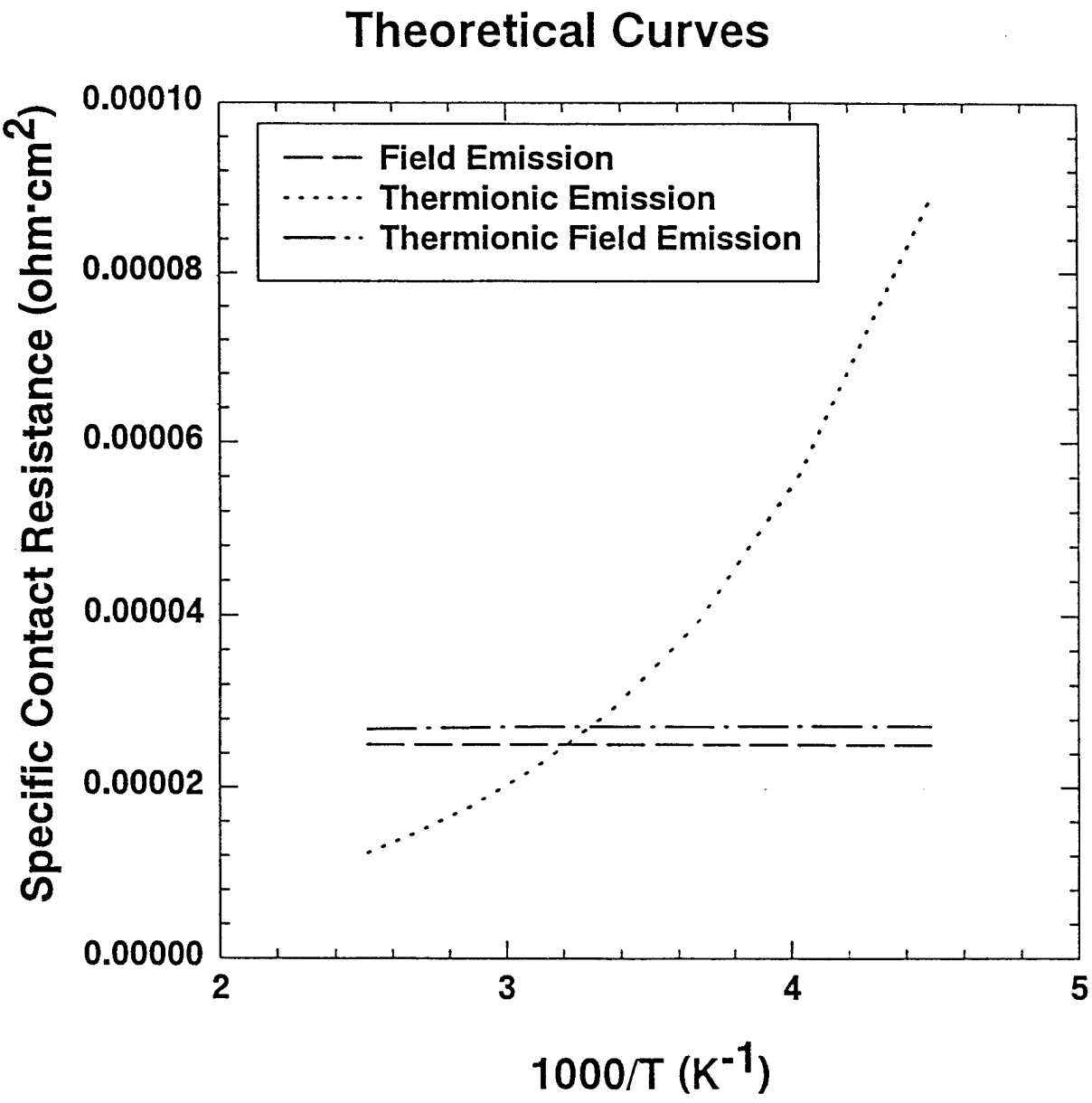

Fig. II.a.7. Theoretical curves for the temperature dependence of specific contact resistance of contacts in which thermionic emission, thermionic field emission, or field emission are the dominant conduction mechanism.

established for m* and ε_s for all the nitride compounds, the best available values for InN were used ($m^* = 0.1 m_e$ and $\varepsilon_s = 8\varepsilon_o$).

Over the temperature range we studied there was little difference between the slope expected for the theoretical field emission and thermionic field emission plots (Fig. II.a.7). The thermionic field emission does have a slight upward slope with increasing reciprocal temperature, but it is less than the error found in the experimental measurements on the samples. By contrast, the thermionic emission case shows an obvious trend over the temperature range.

Fig. II.a.8 (top) shows the temperature dependent contact resistance data for InN contacted with WSi_x. The 500°C annealed contact has approximately constant contact resistance over this temperature range, as is expected for InN with this doping level ($qE_{00}/kT \sim 77$). The contact resistance for the as-deposited contact, however, rises with temperature, characteristic of thermionic emission. This may be a result of changing doping levels in the InN because of the sputter deposition of the contact, as is the case for GaAs. The specific contact resistance of InN contacted with W as-deposited and after a 500°C anneal was also measured (Fig. II.a.8 middle). Again the annealed contact shows a relatively constant contact resistance over the range while the as-deposited contact shows an upward trend. Temperature dependent contact resistance values for InGaN contacted with W and WSi_x are shown in Fig. II.a.8 bottom. The specific contact resistance is very low ($< 10^{-5}\ \Omega \cdot cm^2$) for both metals. There is no clear pattern to the data over this temperature range. There is however no upward trend that would indicate thermionic emission. For this material, the value of E_{00} was estimated to be 0.63 eV based on doping levels. This gives a value of $qE_{00}/kT \sim 24$ indicating field emission conduction is expected to be dominant.

In summary, W, WSi_x and Ti/Al were found to produce low resistance ohmic contacts on n^+ InGaN and InN and InAlN. W contacts proved to be the most stable, and also gave the lowest resistance to InGaN and InN, $\rho_c < 10^{-7}\ \Omega \cdot cm^2$ after 600°C anneal, and $1 \times 10^{-7}\ \Omega \cdot cm^2$ after 300°C anneal, respectively. The contact resistance stability varied for each material and degraded at temperatures > 400°C on InN, ≥ 600°C on InGaN, while those on InAlN were not stable. WSi_x contacts to InN graded from $In_{0.6}Al_{0.4}N$ had $\rho_c \sim 10^{-5}\ \Omega \cdot cm^2$ after a 500°C anneal, over a order of magnitude lower than WSi_x contacts directly to In0.6Al0.4N. Theoretical calculations based on the doping levels of InGaN and InN indicate that the dominant conduction mechanism in W-based ohmic contacts to these materials should be field emission. The experimental data fit curves for field emission or thermionic field emission for InGaN contacted with WSi_x and W. InN samples contacted with both W and WSi_x showed similar behavior after annealing at 500°C, while for as-deposited the curves fit better to the thermionic emission case. This may indicate that the deposition of the contact metal lowered the doping levels in the InN, while annealing returned them to a higher level.

II.b. Dry Etching - Plasma Etching of III-Nitrides in ICl/Ar and IBr/Ar Plasmas

Dry etching of GaN and related compounds in various chemistries have been investigated in both reactive ion etching, (RIE), and electron cyclotron resonance (ECR) modes. ECR etching has proven much more efficient than RIE for the nitrides due to higher ion and excited neutral densities and more effective bond-breaking, allowing the etch by-products to form more readily. Another concern is preferential loss of the group V element from the surface

Fig. II.a.8. Experimentally determined, temperature-dependent specific contact resistance values for InN contacted with WSi_x (top) and W (middle), and for InGaN contacted with W and WSi_x (bottom).

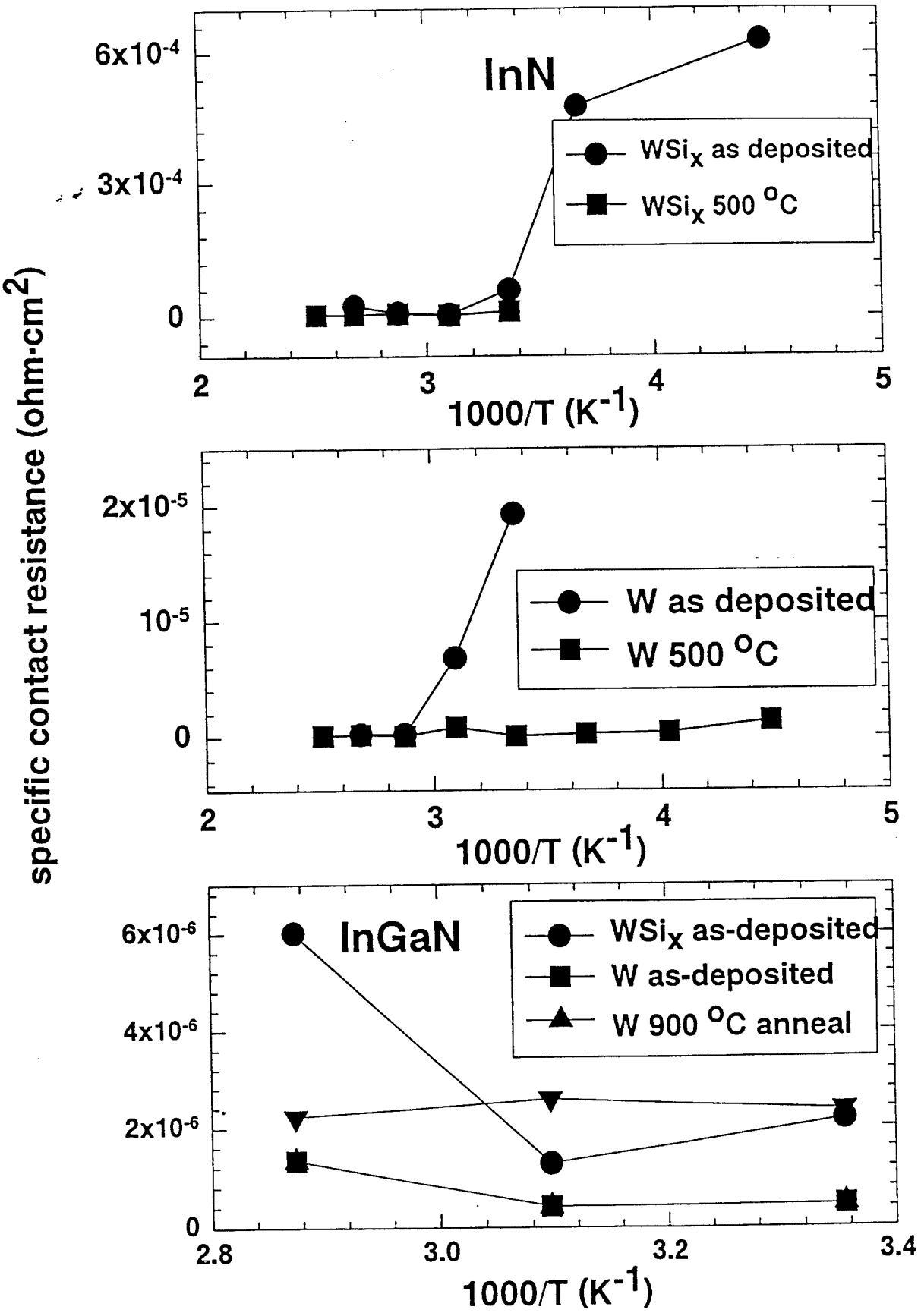

due to its higher volatility, which can result in rough morphologies during etching of compound semiconductors. This is of particular concern for the nitrides. The dry etching of III-V materials is often rate limited by removal of the group III etch product, particularly for In-containing materials. Various alternative plasma chemistries have been explored in the search for a fast, smooth, anisotropic etch for nitrides, such as Br_2 and I_2. Pearton et al. investigated the ECR etching of InP in $HI/H_2/Ar$ and found etch rates > 1 μm/min, smooth anisotropic etching with no residue after etch. This chemistry was also used to etch GaAs, InAs, InSb, InP, and GaSb, reporting features that were anisotropic, smooth, with no deposition during etch, and an order of magnitude faster rates than with the $CH_4/H_2/Ar$ chemistry. Less work has been done with Br_2-based plasma discharges. GaN has been etched in HBr, HBr/Ar, and HBr/H_2 under reactive ion etch conditions, with etch rates around > 600Å/min at 400 V dc. Somewhat faster rates were achieved under ECR conditions in HBr/H_2 (~900Å/min at -150 V dc). Plasma chemistries based on ICl and IBr are of interest as plasma dissociation produces active chlorine or bromine and iodine and should provide efficient etching of the nitrides. A review of nitride etching results has recently appeared. In this paper we report experiments comparing ICl/Ar and IBr/Ar ECR plasma etching of GaN, InN, InAlN, AlN and InGaN.

The GaN, AlN, InN, $In_{0.36}Al_{0.64}N$ and $In_{0.5}Ga_{0.5}N$ samples were grown by Metal Organic Molecular Beam Epitaxy (MOMBE) on semi-insulating, (100) GaAs and Si substrates or on Al_2O_3 substrates in an Intevac Gen II system as described previously. The group-III sources were triethylgallium, trimethylamine alane and trimethylindium, respectively, and the atomic nitrogen was derived from an ECR Wavemat source operating at 200 W forward power. The layers were single crystal with a high density of stacking faults and microtwins. The GaN and AlN were resistive as-grown, and the InN was highly auto-doped n-type ($>10^{20}$ cm^{-3}) due to the presence of native defects. InAlN and InGaN were found to contain both hexagonal and cubic forms. The $In_{0.36}Al_{0.64}N$ and $In_{0.5}Ga_{0.5}N$ compositions we employed were conducting n-type as grown (~ 10^{19} cm^{-3}) due to residual auto-doping by native defects.

The samples were patterned with either a carbon-based mask or photoresist, and were etched in a Plasma-Therm SLR 770 reactor with an Astex 4400 low profile ECR source. The ICl and IBr are crystalline solids with melting temperatures of ~ 23 and 50°C respectively. We loaded ~ 50 g of ICl or IBr into a stainless steel vacuum vessel directly connected to a mass flow controller which injected the vapor into the ECR source. The vacuum vessel was wrapped in Al-foil and heated to ~ 45°C. We obtained flow rates up to 12 standard cubic centimeters per minute (sccm). The process pressure was held constant at 1.5 mTorr and the temperature of the He back-side cooled chuck was held at 23°C. The rf power (13.56 MHz) was varied between 50 and 250 W and the microwave power between 400 and 1000 W. The plasma chemistries used were ICl/Ar or IBr / Ar with respective flows of 4 sccm/4 sccm, 2 sccm/ 6 sccm, 1 sccm/ 7 sccm and 8 sccm/ 0 sccm. Step heights were obtained from Dektak stylus profilometry measurements after the removal of the carbon mask with acetone, and used to calculate the etch rates. The error in these measurements is approximately ± 5%. The surface morphology of selected GaN samples were examined with Atomic Force Microscope (AFM) using a Si tip in tapping mode and Scanning Electron Microscopy (SEM), while near-surface composition was measured by Auger Electron Spectroscopy (AES).

The etch rates as a function of plasma composition for GaN, InN, InAlN, AlN and InGaN are shown in Fig. II.b.1. Microwave power was held at 1000 W and rf power at 150 W

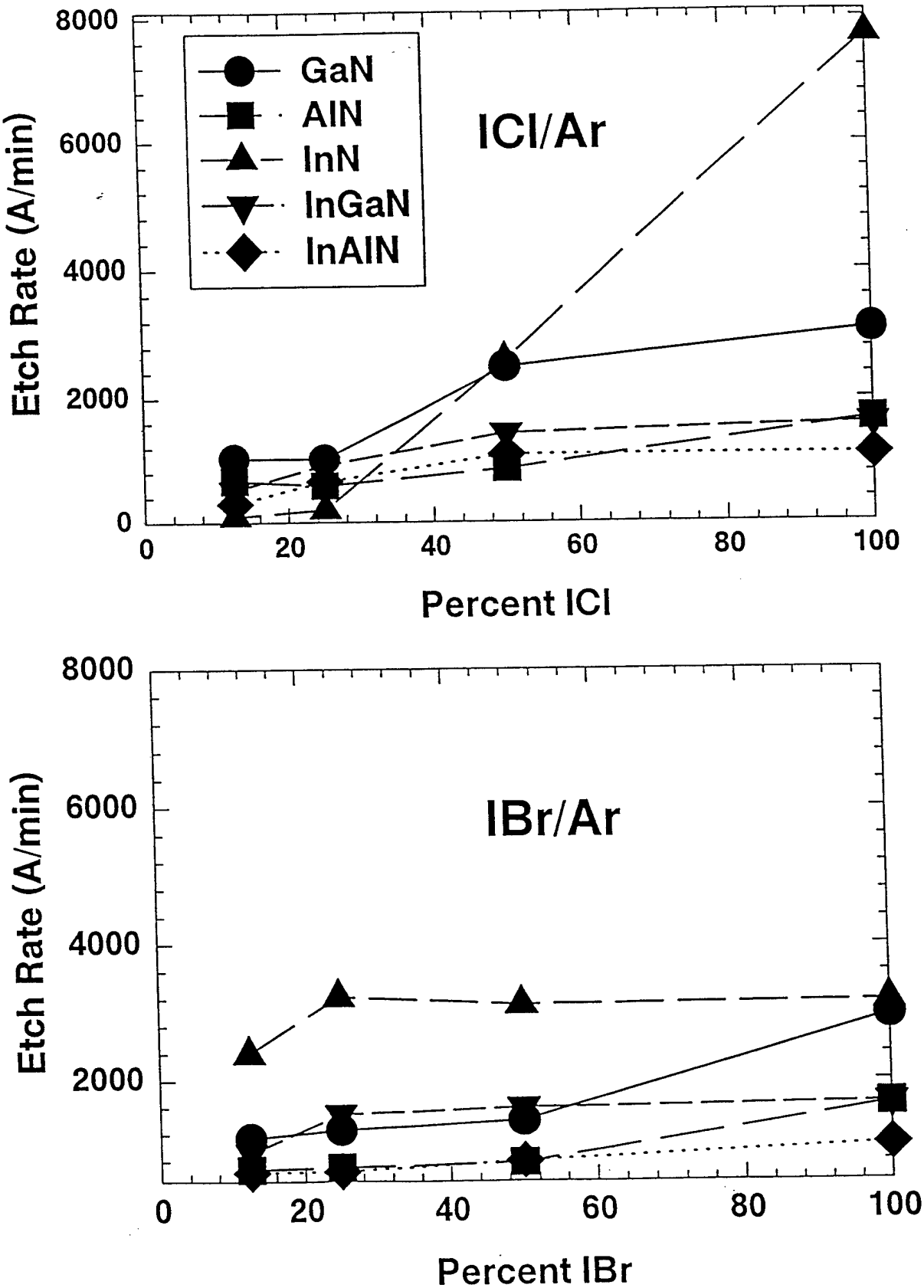

Fig. II.b.1. Etch rate as a function of percent ICl (top) or IBr (bottom) for GaN, InN, InAlN, AlN and InGaN in 1000 W (ECR), 150 W rf, 1.5 mTorr discharges.

(corresponding to a dc self bias of -170 V at the sample position). For the ICl based etch (Fig. II.b.1, top), the GaN and InGaN etch rates rise as the amount of ICl in the etch increases from 12.5 to 50%, and then level off. Above 50% ICl there appears to be a competition between the formation of $GaCl_3$ with has a boiling point of 201°C, with that of GaI_3 which sublimes at 345. The $GaCl_3$ may form preferentially at some plasma compositions. The InN shows a sharp increase in etch rate above 25% ICl. This suggests that at 25% ICl the InI_3, which is much more volatile ($InCl_3$ boils at 600°C, InI_3 at 210°C), can form easily. The InAlN and AlN are not greatly effected by changes in the composition of the plasma in ICl (or IBr, Fig. II.b.1, bottom), perhaps because both Al containing etch products have similar volatility ($AlCl_3$ boils at 183°C, $AlBr_3$ at 263°C and AlI_3 at 191°C) and because the etch rate is probably limited by the initial bond breaking in the Al-containing materials. We expect that AlN and InAlN will be difficult to etch because of their high average bond energies (11.52 eV/atom for AlN, 7.72 eV/atom for InN, compared to 6.52 eV/atom for GaAs). The N containing etch products are much more volatile than the group-III etch products, with NCl_3 boiling at < 71°C while NI_3 is explosive.

The etch rates for InN and InGaN increased as the amount of IBr in the etch increased from 12.5 to 25%, and remained constant at higher percentages (Fig. II.b.1, bottom). This suggests that above 25% IBr the etching is no longer reaction-limited. The $InBr_3$ etch product is much less volatile than InI_3, as mentioned earlier. Above that composition however, there may have been competition between the formation of $InBr_3$ and InI_3, which slowed the etch, or the etch may have been limited by the removal of the reactants from the surface. GaN etch rates showed little change with IBr composition to 50% IBr plasma composition, but at 100% IBr the etch rates increased sharply. There may not have been enough reactants at the etch surface at 50% IBr, or at these lower percents of IBr there may be a competition between the formation of $GaBr_3$ and GaI_3.

In Fig. II.b.2 the etch rate as a function of microwave power for GaN, InN, InAlN, AlN and InGaN is shown for values between 400 and 1000 W for ICl/Ar plasmas (top) and IBr/Ar (bottom). The rf power was held at 150 W, and 4 sccm ICl or IBr / 4 sccm Ar gas flows were used. Both InAlN and AlN have low etch rates in ICl/Ar, and show no significant change in etch rate with increasing microwave power. This indicates that they are not reaction limited in this chemistry, since increasing the microwave power results in a higher concentration of reactive species which enhances the chemical component of the etch mechanism. GaN and InGaN showed a slight increase in etch rate from 400 W microwave power to 600 W. Thereafter the GaN etch rate dropped gradually with increasing microwave power, while the InGaN etch rate dropped sharply at 800 W and then remains constant at 1000 W. This would indicate either a diffusion-limited etch, where the number of reactants becoming available exceeds the rate at which the iodine and/or chlorine etch products can be removed, or competition between reactants occurs above 600 W microwave power. The InN had a maximum in etch rate at 800 W ECR power. This might result from the large difference in volatilities of the etch products for this material, leading to a strong sensitivity to reactant density. We expect that below that density the etch rate is reaction-limited and above it there is competition between the reactants that limits the etch rate. A similar trend is observed for InN in the IBr/Ar mixtures although the peak is not as distinct.

The etch rates for InAlN and AlN were again quite low in IBr based plasmas (Fig. II.b.2, bottom). GaN had constant etch rates for powers between 400 W and 800 W in the IBr

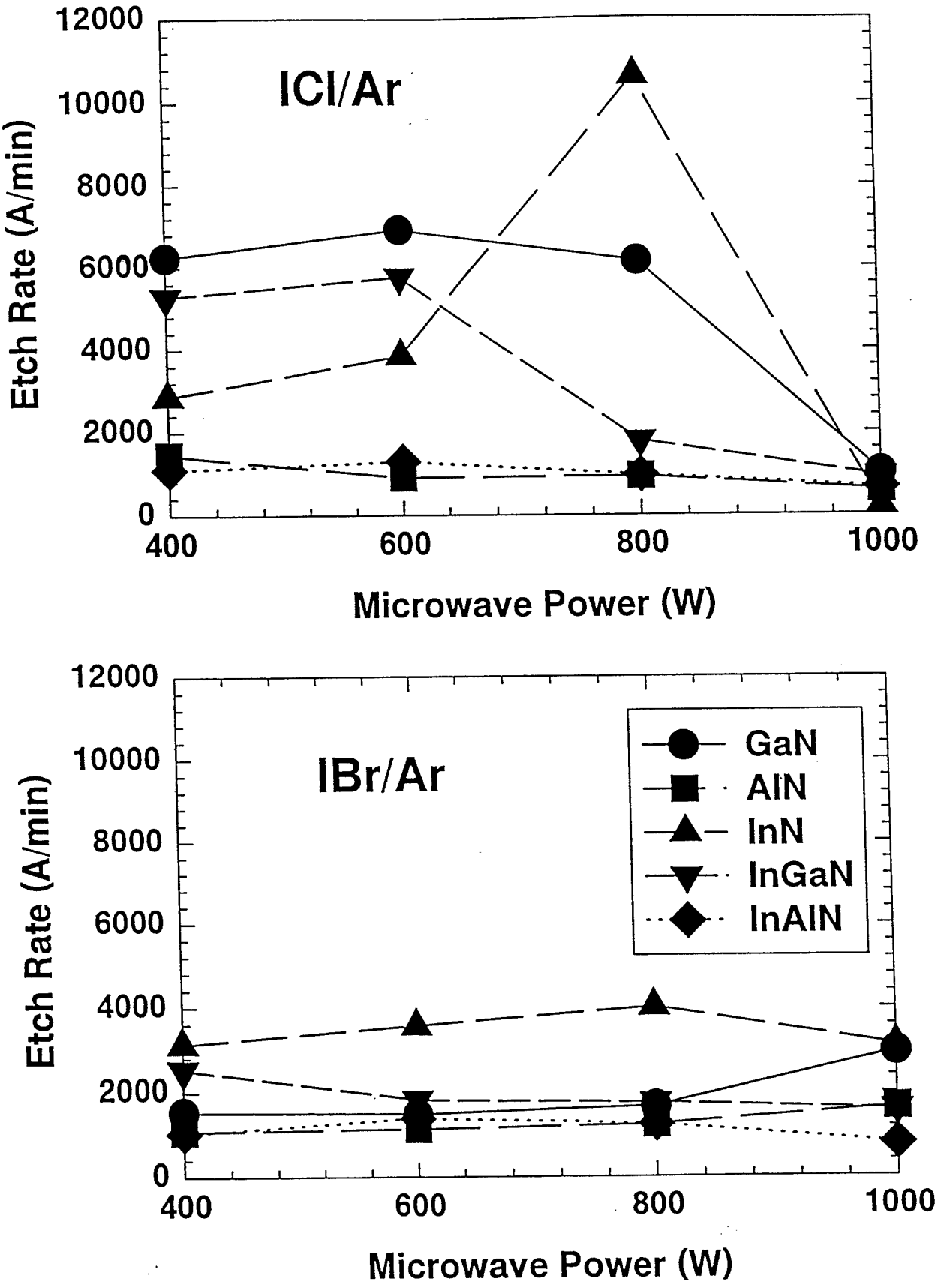

Fig. II.b.2. Etch rate as a function of microwave power for GaN, InN, InAlN, AlN and InGaN in 4 ICl/4 Ar (top) or 4 IBr/4 Ar (bottom) plasmas (150 W rf, 1.5 mTorr).

chemistry, and then increased sharply at 1000 W. The InGaN etch rate again decreased with increasing microwave power. As the InGaN etch rate increased monotonically with increasing rf power (as will be seen shortly), the removal of the etch products would seem to be limiting the etch rates for this material.

Fig. II.b.3 shows the etch rate as a function of rf power for GaN, InN, InAlN, AlN and InGaN in ICl/Ar (top) and IBr/Ar (bottom) plasmas for chuck powers between 50 and 250 W. Microwave power was held at 1000 W and the flow was held at 4 sccm ICl or IBr / 4 sccm Ar. The AlN and InAlN rates were affected very little by increasing rf power in either chemistry. GaN, InN and InGaN all have large increases in etch rate as the rf is increased from 150 to 250 W in the ICl chemistry. This could mean that the bombarding ions have enough energy to remove the less volatile etch product at this power or to more efficiently break bonds, allowing the etch to proceed with both I- and Cl- etch products. GaN etch rates in IBr/Ar increased with increased rf power to 150 W, and then decreased slightly at 250 W, where the sputtering ions may have removed reactants before the etch could proceed. InN and InGaN in IBr/Ar plasmas had large increases in etch rate as the rf was increased from 150 to 250 W, similar to the results in ICl/Ar.

In Fig. II.b.4 the RMS roughness for GaN etched in ICl/Ar as a function of rf power is shown. The RMS roughness for the as grown sample is shown for reference. These samples were unpatterned to avoid roughness caused by mask material being redeposited. The etched surfaces were found to be significantly smoother than that of the as grown sample indicating that surface features are removed predominantly by sputtering. Sharp features will be removed by ion milling faster than flat features because of the angular dependence of milling rate, and as long as preferential sputtering of N does not occur, this will lead to a degree of smoothing of the surface. Above 150 W the surface roughness begins increasing again, probably due to the onset of preferential sputtering.

AES depth profiles of GaN as-grown and etched in ICl/Ar at 50 W or 100 W rf power are shown in Fig. II.b.5. At these powers we find no reduction in the N/ Ga ratio. This means that there is little preferential loss of N during the etching at these powers. Adventitious C and O from native oxide are also observed on the surface of these samples. I and Cl are found in the top 25Å of the etched samples. Similar results were found for GaN etched in IBr/Ar plasma, though no Br was detected on the surface. At high rf powers one would expect preferential N-loss, as reported previously by Shul et. al.

Fig. II.b.6 shows the etch selectivity of GaN over InN, InAlN, InGaN or AlN under ICl/Ar conditions as a function of rf power (top), percent ICl (middle) and microwave power (bottom). The selectivity of GaN over the other nitrides rose with increasing rf power, with GaN/AlN reaching ~ 6 and GaN/InAlN almost 5 at 250 W rf. The volatility of the $InCl_3$ was lower than that of $GaCl_3$, and as the percent ICl in the etch increased, so did the selectivity for GaN/InN, reaching ~ 10 at 100% ICl. With both $GaCl_3$ and GaI_3 having high volatilities, with increasing reactant concentration, GaN was etched faster than the In-containing compounds, which may still be limited by removal of $InCl_3$. GaN etched much faster than AlN and InAlN as well for most microwave powers (Fig. II.b.6, bottom), achieving selectivities of ~8 and 5 respectively at 600 W microwave power. In IBr/Ar chemistries the selectivities were low, as shown in Fig. II.b.7, never going above 4 for any set of rf or microwave powers of plasma compositions. We assume this is due to the similar volatilities of iodide and bromide etch products.

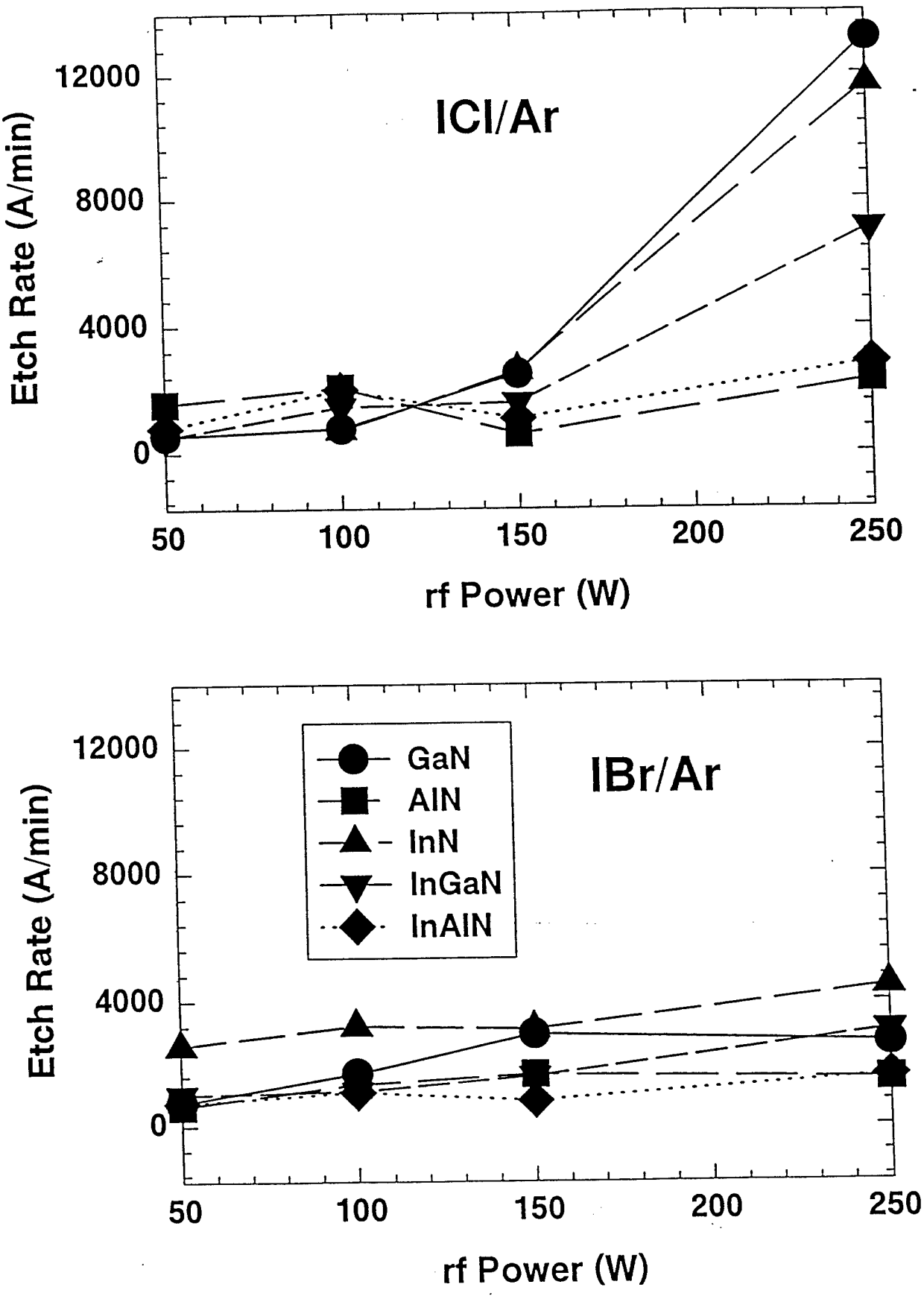

Fig. II.b.3. Etch rate as a function of rf power for GaN, InN, InAlN, AlN and InGaN in 4 ICl/4 Ar (top) or 4 IBr/4 Ar (bottom) plasmas (1000 W ECR, 1.5 mTorr).

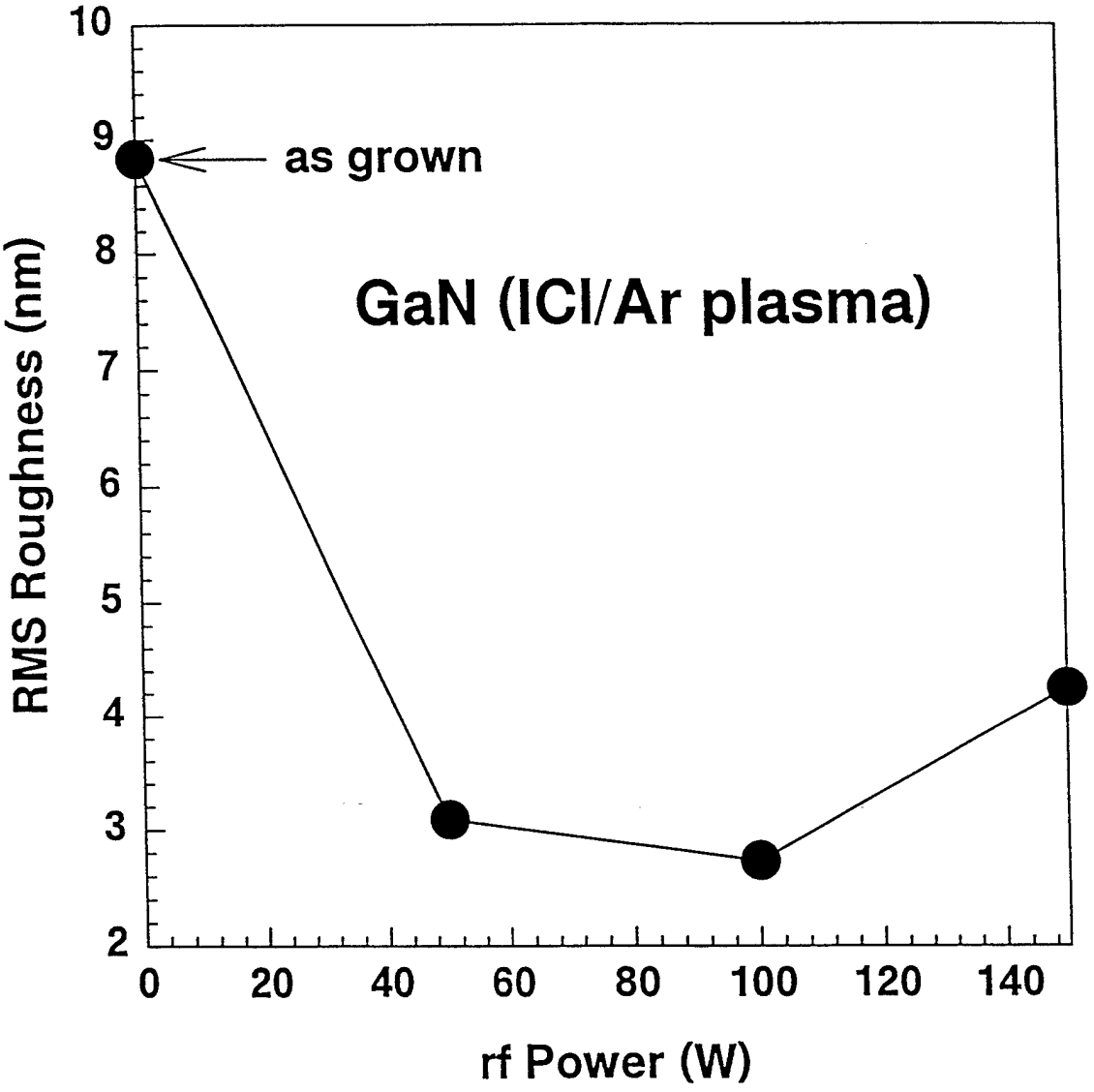

Fig. II.b.4. RMS roughness for GaN as a function of rf power in 4 ICl/4 Ar 1000 W ECR, 1.5 mTorr discharges plasmas.

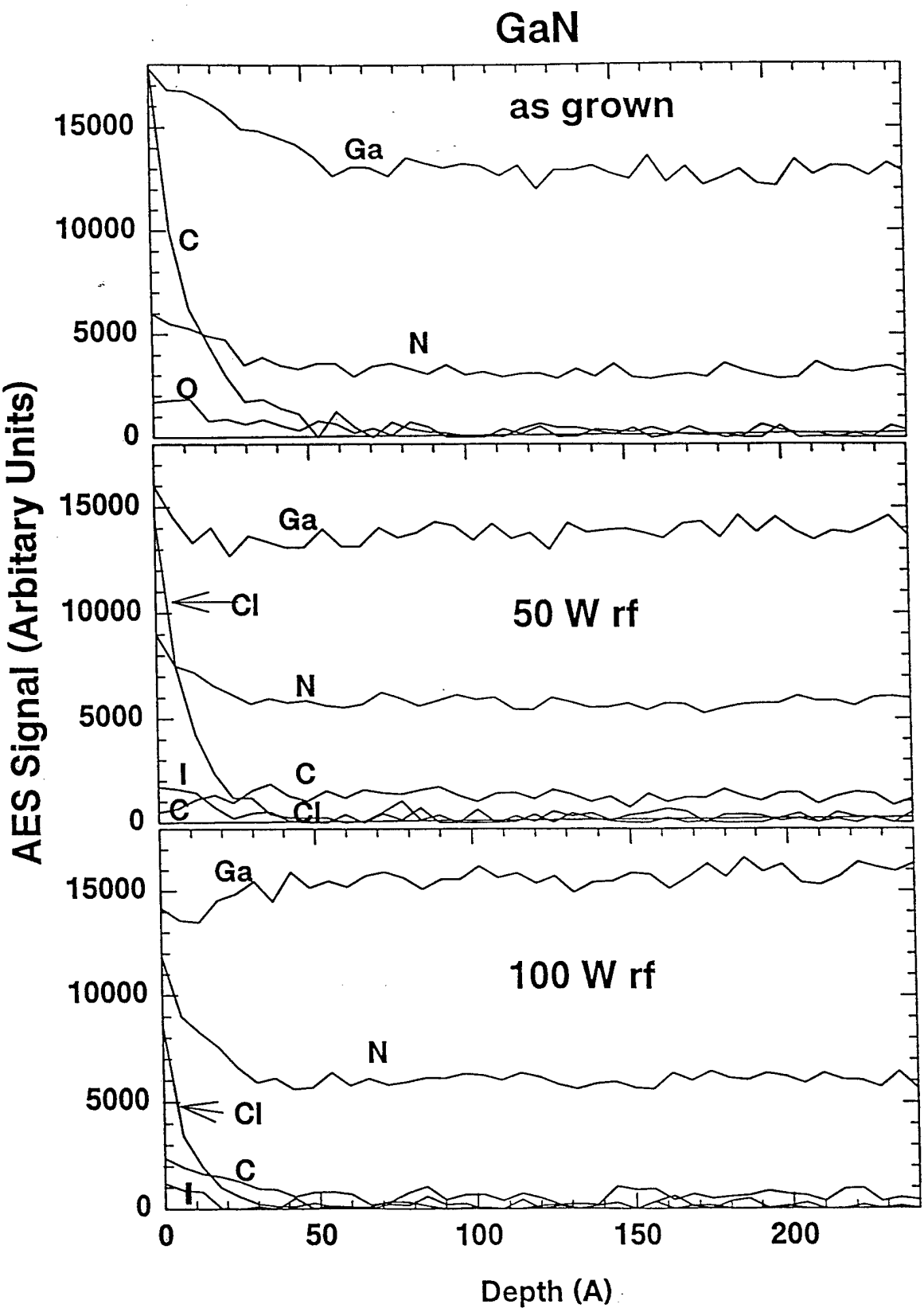

Fig. II.b.5. AES depth profiles of GaN as-grown (top), and etched in 4 ICl/ 4 Ar at 50 W rf (middle) and at 100 W rf (bottom) power. The ECR source power was 1000 W and the pressure 1.5 mTorr.

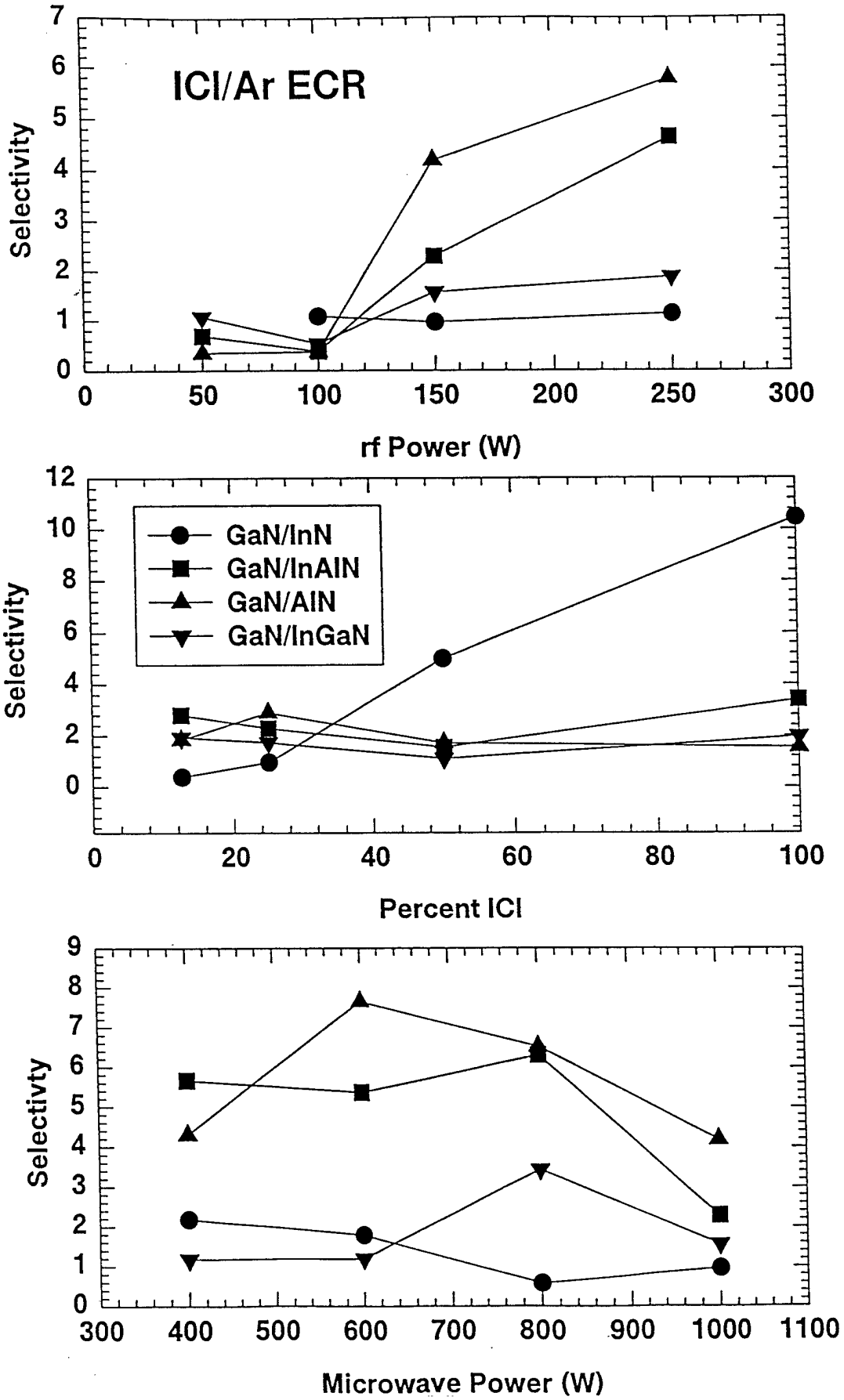

Fig. II.b.6. Selectivity of GaN over InN, InAlN, InGaN or AlN in ICl/Ar plasmas as a function of rf power (top), percent ICl (middle) and microwave power (bottom). The ECR power was 1000 W for the top two plots, the rf power 150 W for the bottom two plots and the plasma composition 4 ICl/4 Ar for the top and bottom plots.

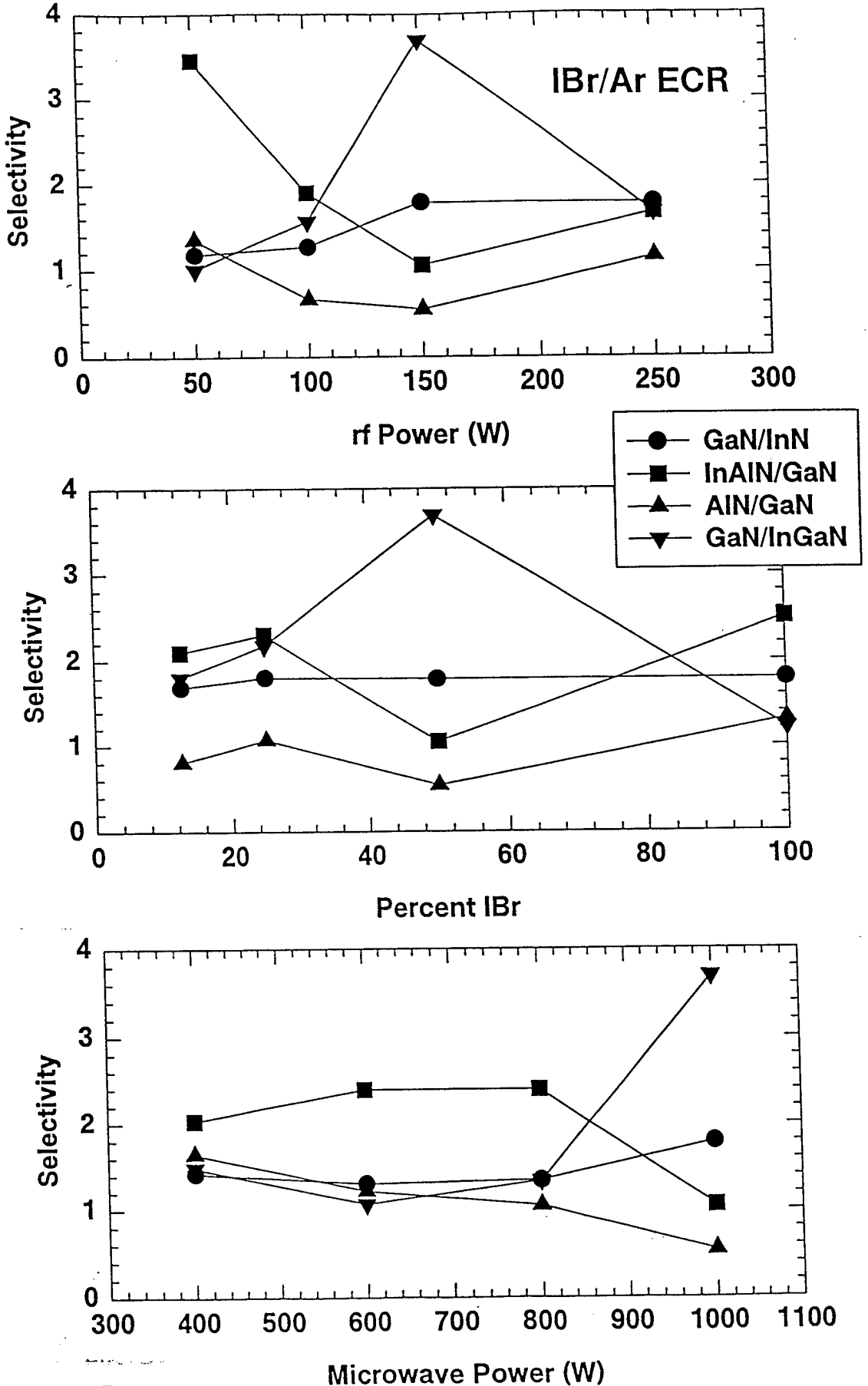

Fig. II.b.7. Selectivity of GaN over InN, InAlN, InGaN or AlN under IBr/Ar plasmas as a function of rf power (top), percent ICl (middle) and microwave power (bottom). The ECR power was 1000 W for the top two plots, the rf power 150 W for the bottom two plots and the plasma composition 4 ICl/4 Ar for the top and bottom plots.

The etch rates for GaN, InN, InAlN, AlN and InGaN were measured in ICl/Ar and IBr/Ar plasmas. The sensitivity to changes in plasma chemistry, microwave power and rf power appears to be directly influenced by the volatility of the group-III -I and Cl- or Br-etch products. InN, with the largest difference between volatility of etch products, proved to be the most sensitive to the plasma composition and ion density in ICl/Ar plasma chemistries. Very fast etch rates were achieved for GaN, InN and InGaN in ICl/Ar chemistries. At 250 W rf power AlN and InAlN had slow etch rates in this mixture and were affected very little by changes in etch conditions. GaN and AlN etched in IBr/Ar showed a sharp increase in etch rate as the IBr composition increased from 50 to 100%, while the etch rates for the other materials stayed relatively constant above 25% IBr. All the materials showed a general increase in etch rate with increasing rf power in both chemistries. The etched surface of GaN under both plasma chemistries was found to be extremely smooth with little preferential loss of N from the surface at low rf powers. There was no detectable residue from the etch after IBr/Ar plasma, and only slight Cl residue in ICl/Ar chemistry. Selectivity of GaN over InN, InAlN, InGaN or AlN in ICl/Ar plasmas as a function of rf power (top), percent ICl (middle) and microwave power (bottom). The ECR power was 1000 W for the top two plots, the rf power 150 W for the bottom two plots and the plasma composition 4 ICl/4 Ar for the top and bottom plots.

(III) Ohmic Contacts to p-GaN (Paul Holloway and Jeff Trexler)

Studies continued this quarter emphasizing the search for a contact metallization to replace the previously studied Au/Ni contact scheme. Both Pd and Cr were deposited in place of Ni in the hope that one of these elements would react with the underlying GaN to provide for the possibility of increased doping in the near surface region of the semiconductor which will allow for a greater probability for tunneling to occur resulting in low resistance ohmic contacts. The p-GaN:Mg substrates used had a carrier concentration of 9.8×10^{16} cm^{-3}. All contacts were deposited by electron beam evaporation with a thickness of 1000Å Au, and 500Å Pd or Cr. The contacts were heat treated up to 600°C for up to 30 minutes in flowing N_2 with current-voltage (I-V) measurements being taken after each anneal. Auger electron spectroscopy (AES) was performed on many of the samples to determine interfacial reactions between the contact metals and the underlying GaN. Temperature dependent I-V measurements were taken for the Au/Pd/GaN contacts following a 600°C for 30 minute heat treatment to determine the dominant conduction mechanism.

Deposition of Au/Pd and Au/Cr provided rectifying but nearly linear I-V curves. Upon heat treatment of the Au/Pd contacts to 200°C an increased resistance was seen. However, following a 400°C heat treatment the potential offset decreased but the curve remained rectifying. I-V curves for all these heat treatments can be seen in Fig. III.1. The I-V curves for the Au/Cr contacts as-deposited were similar in magnitude to the Au/Pd curve but with a slightly more linear nature.

The purpose of substituting Pd or Cr for Ni in the Au/Ni contact scheme is to find a metal that will react with the underlying GaN to a greater extent than Ni, which will provide a greater opportunity for doping of the surface region of the GaN as has been postulated previously. AES depth profiles were used on as-deposited and heat treated samples to determine if any metal/GaN reaction occurred and the extent of this reaction. For the Au/Pd contacts as-deposited, fairly planar interfaces exist between both the Pd:Au and Pd:GaN with no apparent interaction between the Pd/Au contact layer and the underlying p-GaN. Upon heat treatment at 600°C Pd has been shown to react with the Au capping layer forming a

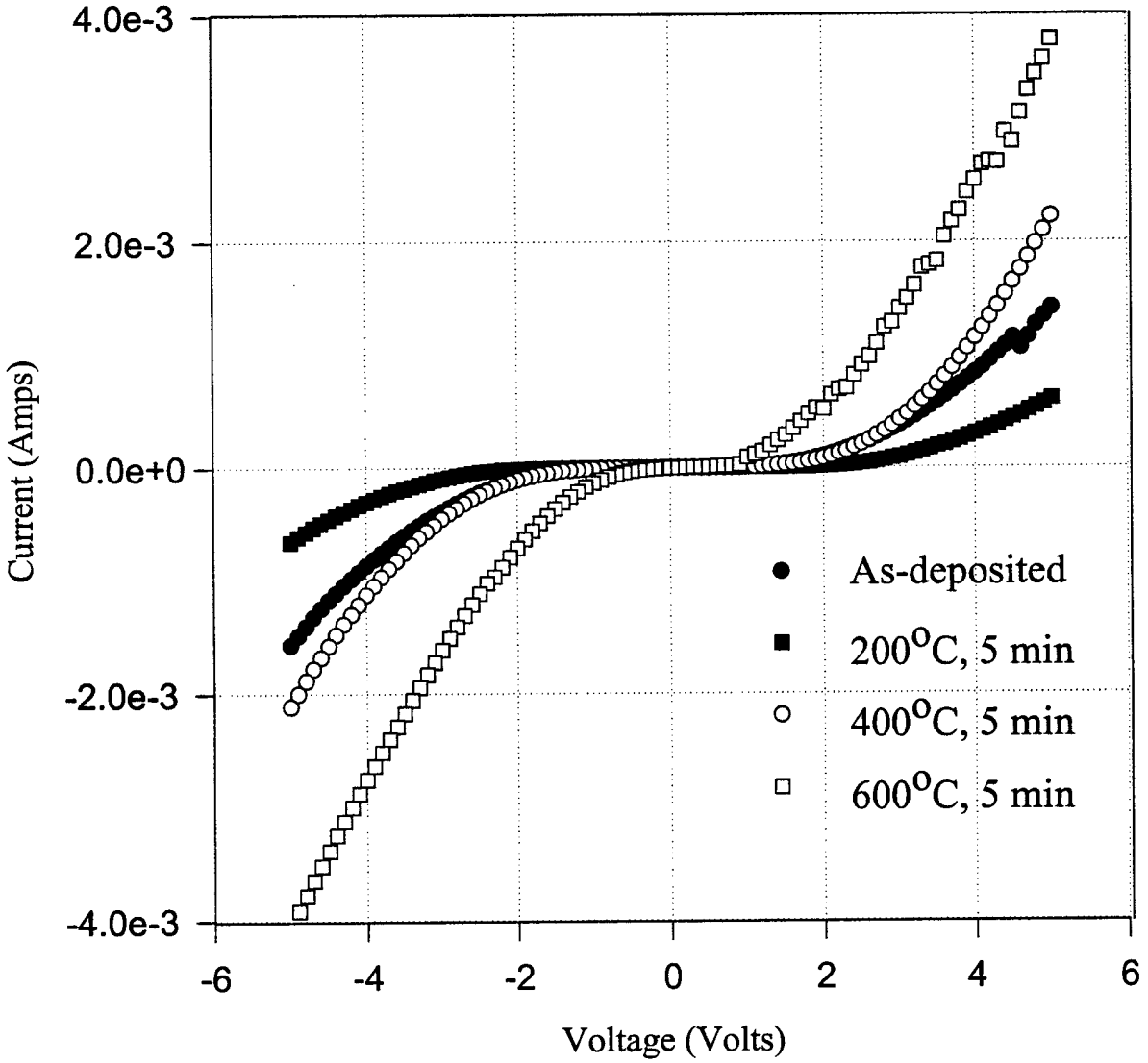

Fig. III.1. I-V curves for Au/Pd/p-GaN.

Au:Pd solid solution (Fig. III.2). It is the formation of this solid solution that is believed to be responsible for the increased conduction in these contacts upon heat treatment. As for the Au/Cr contacts an AES depth profile has been performed on the as-deposited sample showing an abrupt Au/Cr interface and a broadened Cr/GaN interface that may be due to preferential sputtering rates of the crystalline Cr giving a rough interface. (Fig. III.3) Additional depth profiles on heat treated samples are planned to further investigate if there is a reaction between Cr and GaN.

Preliminary indications from the temperature dependent I-V data collected on the Au/Pd contacts annealed at 600°C for 30 minutes are that there is a change in conduction mechanism at about 2.5-3 eV depending on the temperature at which the measurement was taken. It appears that conduction above 2.5 eV is dominated by a tunneling mechanisms (either thermionic field emission or field emission) while at voltages below 2.5 eV thermionic emission is dominating the conduction. Currently these measurements are being performed on Au/Ni and Au/Cr contacts to determine if the conduction mechanisms are similar for those contact schemes.

(IV) Microstructural Characterization of GaN Thin Films Grown on $LiGaO_2$ Substrate (Kevin Jones and Jing Hong Li)

Cross-sectional transmission electron microscope (XTEM) analysis and high resolution transmission electron microscope (HRTEM) have been carried out on GaN thin films MOCVD-grown on a new substrate of single crystalline $LiGaO_2$. The GaN films were grown on the (001) $LiGaO_2$ which has a orthorhombic structure with lattice parameters of a=5.4063 Å, b=6.3786 Å, and c=5.0129 Å, while GaN has a hexagonal structure with lattice parameters of a=3.189 Å and c=5.185 Å. So far two samples (16, 15) were analyzed. The sample 16 was deposited in a low pressure, horizontal cold-wall MOCVD reactor on the (001) $LiGaO_2$ substrate with triethygallium (TEGa) and ammonia NH_3 as precursors and N_2 as carrier gas using a V/III ratio of 3324 and substrate temperature of 850°C under a reactor pressure of 130 Torr for 1 hour. The sample 15 was deposited using similar processing conditions as the sample 16 but using a higher proportion of TEGa, i.e. a lower V/III ratio. The thickness of the GaN films is typically about 0.5 μm.

Fig. IV.1a shows a XTEM micrograph of GaN/$LiGaO_2$ interface and the corresponding selected area diffraction pattern (SADP) with a big aperture from the sample 15. The corresponding SADP (Fig. IV.1b) show that superposition of the GaN $[2\bar{1}\bar{1}0]$ and the $LiGaO_2$ [010] diffraction patterns, suggesting that the GaN film is single crystal and was grown epitaxially on the $LiGaO_2$ substrate. The XTEM micrograph revealed presence of high defect density. The threading dislocation density was high near the interface, but it was reduced with increasing distance from the interface. From Fig. IV.1a, we estimate that the threading dislocation density for sample 15 typically ranges from $10^{10}/cm^2$ near the GaN/$LiGaO_2$ interface, decreasing to $10^8/cm^2$ at a distance of 0.3 μm away from the interface. The dislocation density was determined by estimating the thickness of the TEM foil, and counting the dislocations along a segment parallel to the interface. Contrast analysis shows that there was residual strain at the interface between the GaN and the $LiGaO_2$ substrate, even through the GaN and the $LiGaO_2$ have a very small mismatch of 0.09%. In addition to the diffraction spots, streaking along the [0002] were observed. The streaks are attributed to a basal plane stacking

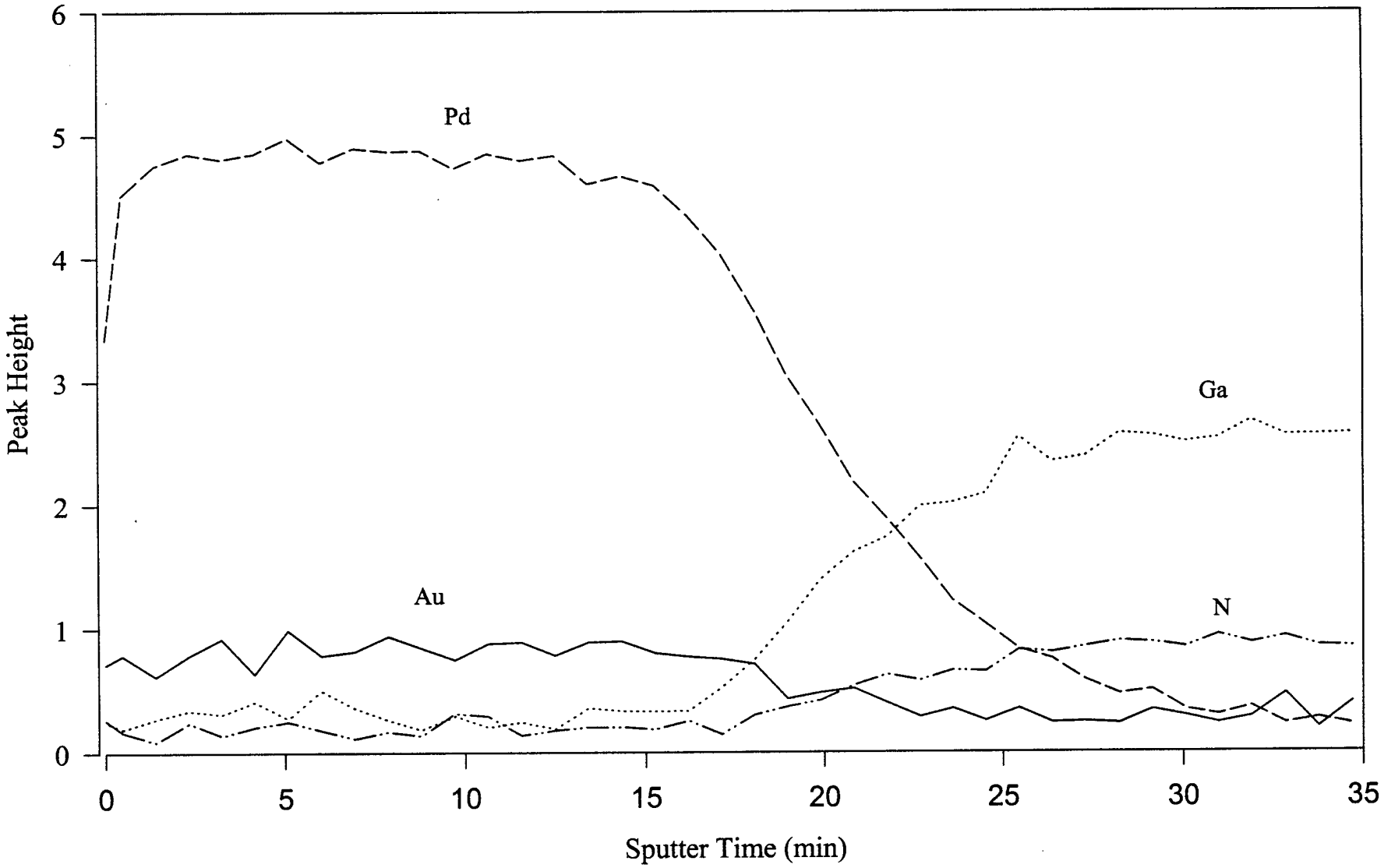

Fig. III.2. AES depth profile of Pd/Au on p-GaN heat treated at 600^{o}C for 30 minutes.

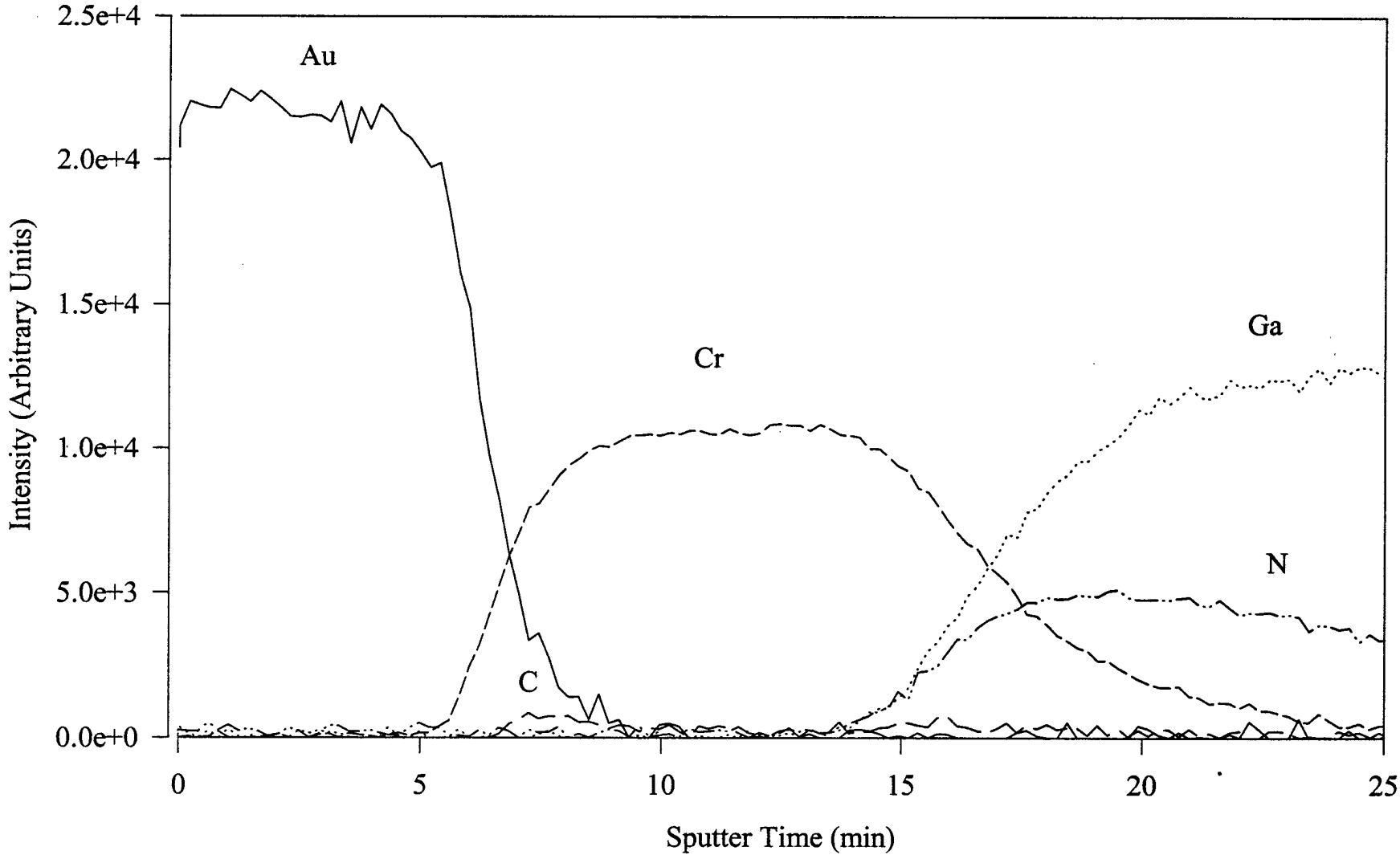

Fig. III.3. AES depth profile of Au/Cr/p-GaN as-deposited.

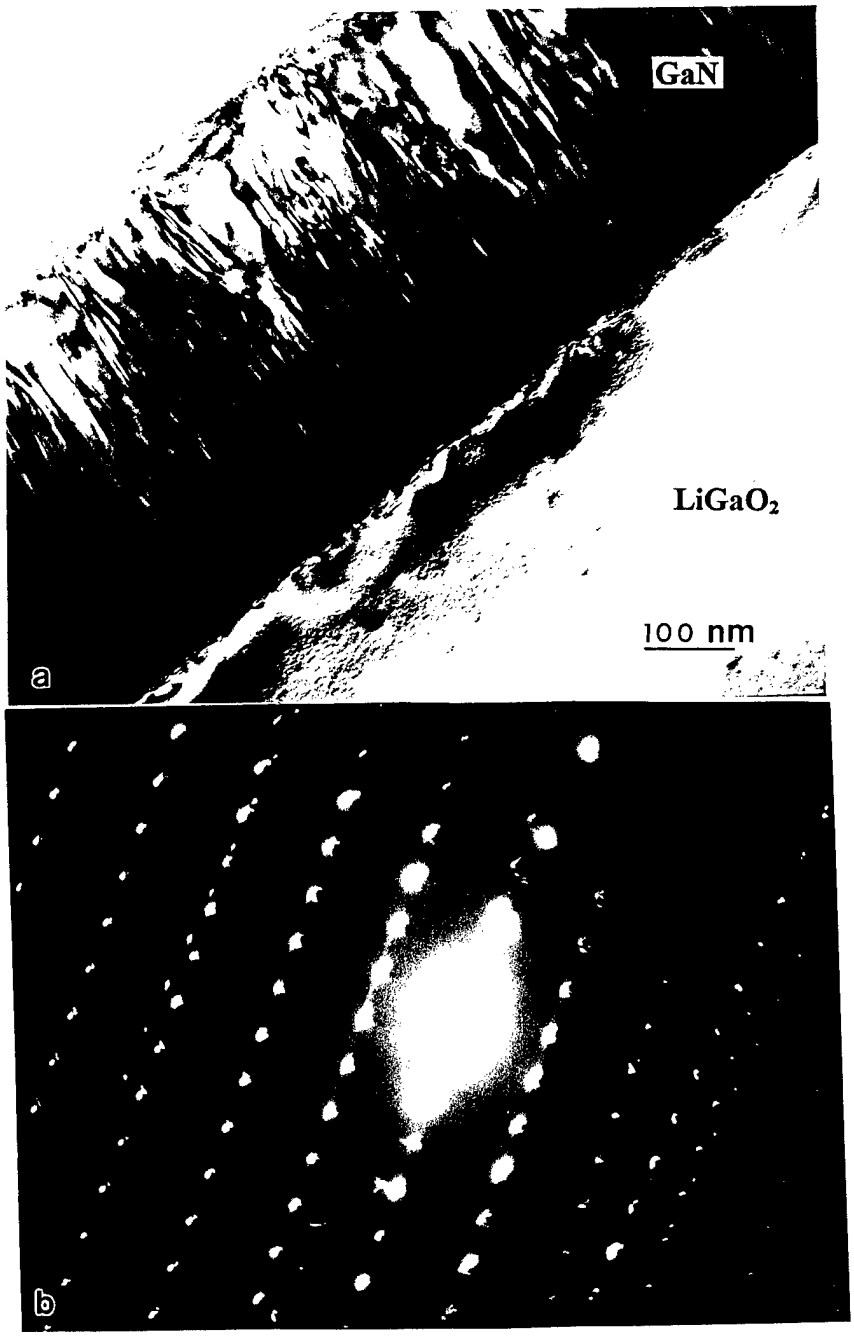

Fig. IV.1a-b.

faults which are parallel to the interface or the LiGaO2 {001} planes. The corresponding SADP (Fig. IV.1b) revealed that the GaN film and the $LiGaO_2$ have the following orientation relationship: $[2\bar{1}\bar{1}0]_{GaN} \parallel [010]_{LiGaO2}$; $(0002)_{GaN} \wedge (002)_{LiGaO2} < 5\text{-}8°$. It was found that the GaN (0002) plane tilted 5-8° from the $LiGaO_2$ (002) plane, as shown in Fig. IV.1b. So the arrangement of the GaN film and the $LiGaO_2$ is shown in Fig. IV.2.

Fig. IV.3 shows a XTEM micrograph of GaN/$LiGaO_2$ interface and the corresponding SADP with a small aperture covered with a half GaN and a half $LiGaO_2$ from the sample 16. Threading dislocations (marked by "d") and stacking faults (marked by arrows) were still observed. Compared with sample 15, it appears that the GaN film of sample 16 has a lower defect density. The threading dislocation density for sample 16 was estimated, ranging from $10^9/cm^2$ at the interface decreasing to $10^7/cm^2$ at a distance of 0.3 μm away from the interface. XTEM micrograph (Fig. IV.3 a) revealed that there is an inter-layer between the GaN film and the $LiGaO_2$ substrate, marked by "A" in Fig. IV.3a. The weak spot-ring in the SADP from the region, as indicated by arrows in Fig. IV.3c, indicates that the inter-layer is amorphous or nano-cyrstalline. This inter-layer might be formed during the film growth at high temperature because of inter-diffusion of N and Li or O, or reaction of the film and the substrate. This kind of inter-layer was found in both samples 15 and 16. This inter-layer may play important role in formation of defects in the GaN film. Chemical compositional analysis of this interlayer will be carried out by either SIMS or EELS.

Dislocation analysis has been conducted by conventional XTEM using the $\vec{g}.\vec{b}=0$ criteria. Fig. IV.4 shows a series of XTEM micrographs taken with different reflections from sample 16 of a $[2\bar{1}\bar{1}0]$ cross-section. The Burger's vectors for some of the threading dislocations were determined to be [0001] and $1/3[11\bar{2}0]$. These dislocations are predominantly edge-type in nature, assuming that the growth direction is the same as the translation vector of the dislocations.

HRTEM has also been carried out on the GaN/$LiGaO_2$. Fig. IV.5 and IV.6 show two HRTEM micrographs of the GaN/$LiGaO_2$ interface for sample 16 and 15, respectively. Both HRTEM micrographs show two dimensional lattice images, both along the GaN $[2\bar{1}\bar{1}0]$ direction. In both cases, plane stacking faults (indicated by arrows) were observed, which were parallel to the GaN/$LiGaO_2$ interface or, the $LiGaO_2$ (001) plane. These plane stacking faults occur at various separations indicating that they are not single polytype stacking order (e.g. 2H, 4H, 6H etc.). They are a mixture of them. Both HRTEM micrographs also confirmed the XTEM observations that there is a nano-crystalline or amorphous inter-layer between the GaN film and the LiGaO2 substrate. A nano-crystalline or amorphous inter-layer has in the past been observed to form in order to relieve stress caused by a big lattice mismatch (~5-10%). However since there is a small lattice mismatch of 0.09%. between the GaN and the LiGaO2, the mechanism driving formation of this layer must be something other than mismatch. Additional HRTEM studies aided with chemical compositional analysis using EDS, SIMS etc will be done to further investigate the cause of the inter-layer, and its impact on the growth of the GaN film.

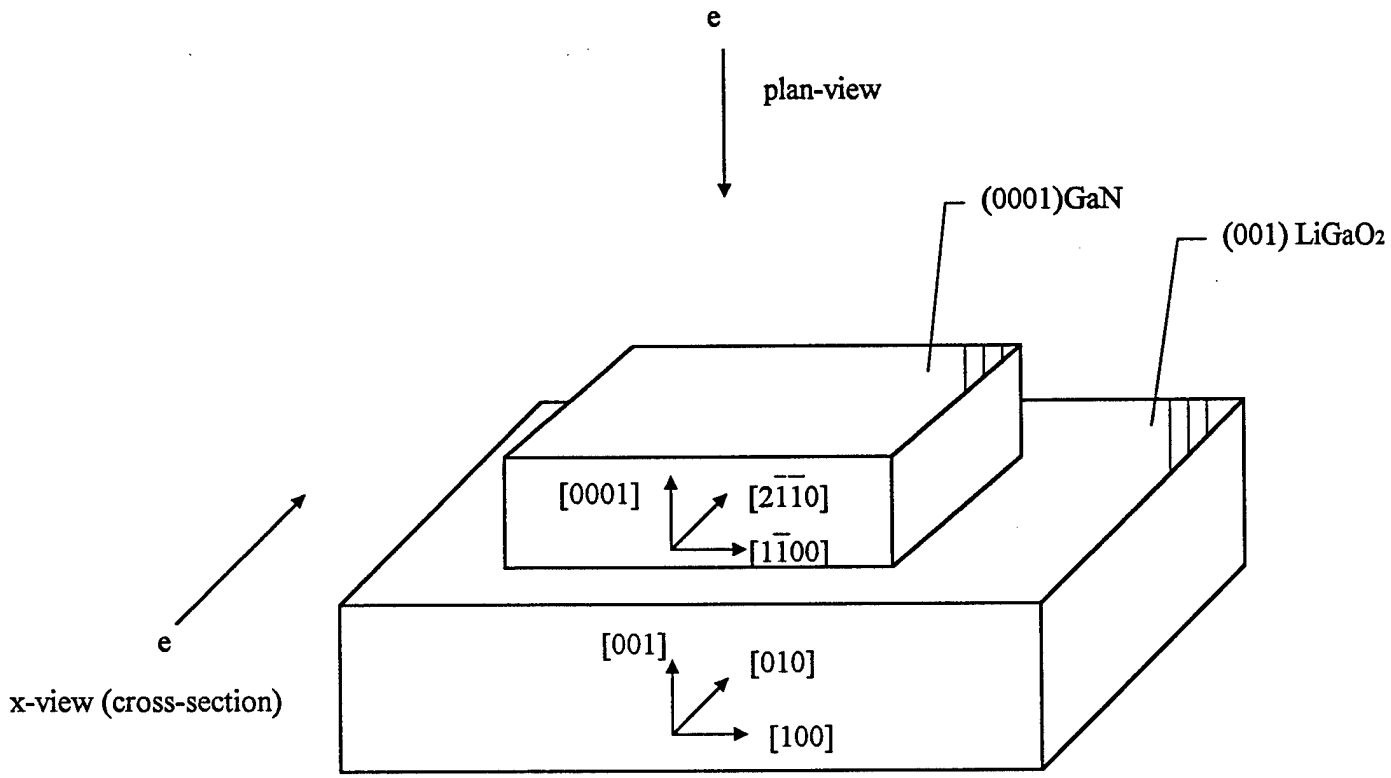

Arrangement of GaN/$LiGaO_2$

Fig. IV.2.

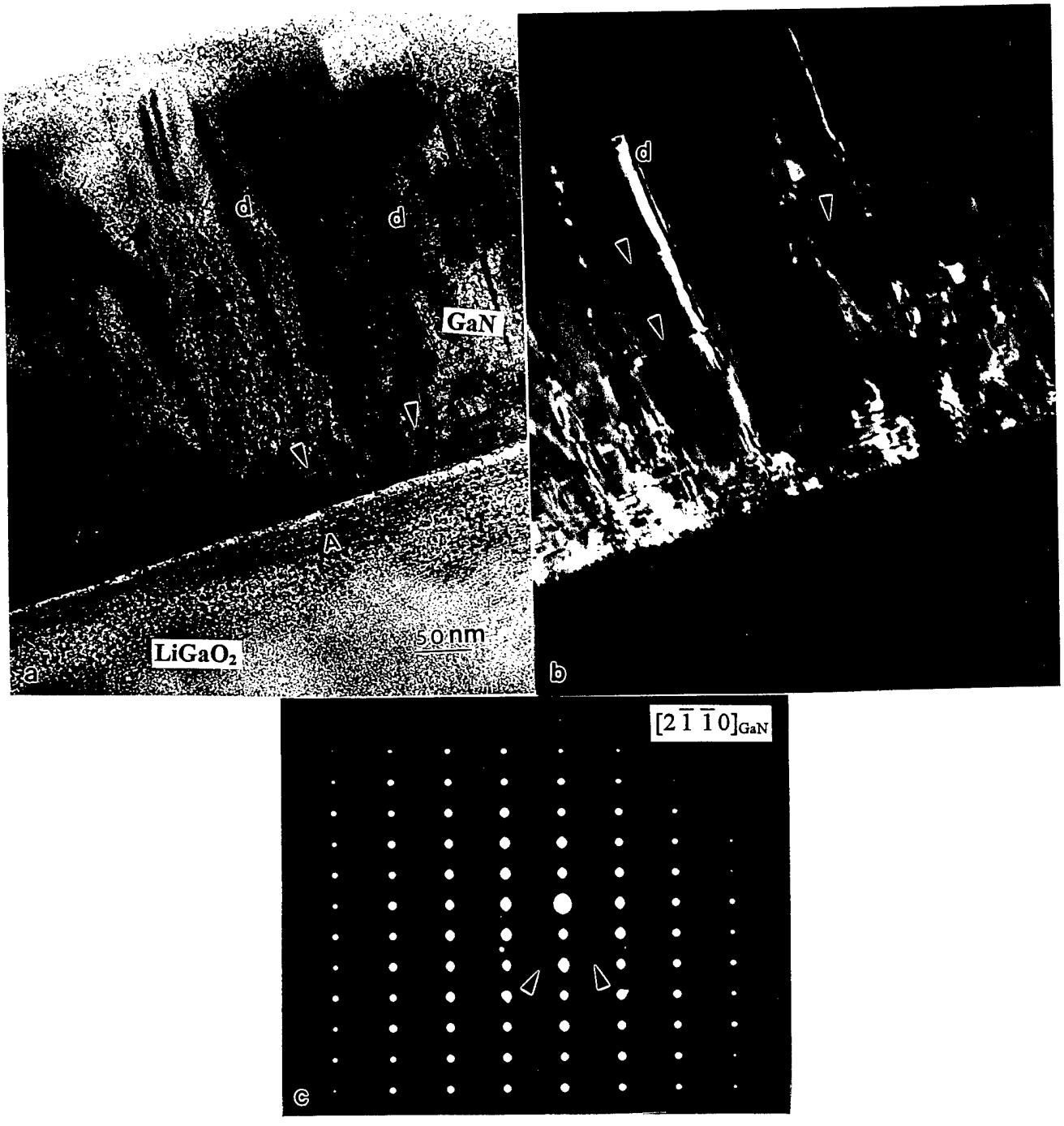

Fig. IV.3a-c.


GaN
LiGaO2
50nm
a
0002
g=0002
b
GaN
LiGaO2
c
1$\bar{1}$00
g=1$\bar{1}$00
d

Fig. IV.4a-d

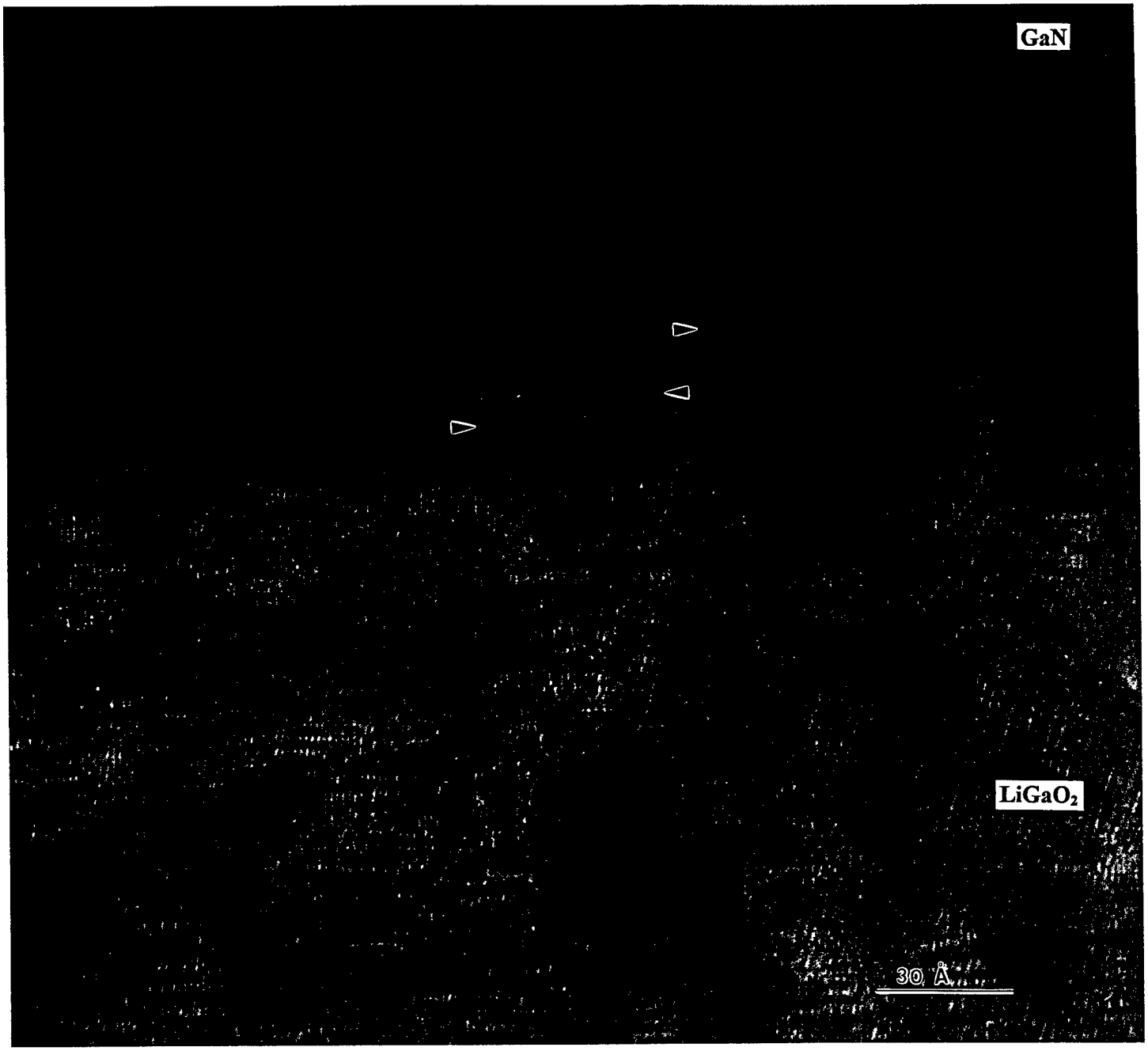

Fig. IV.5

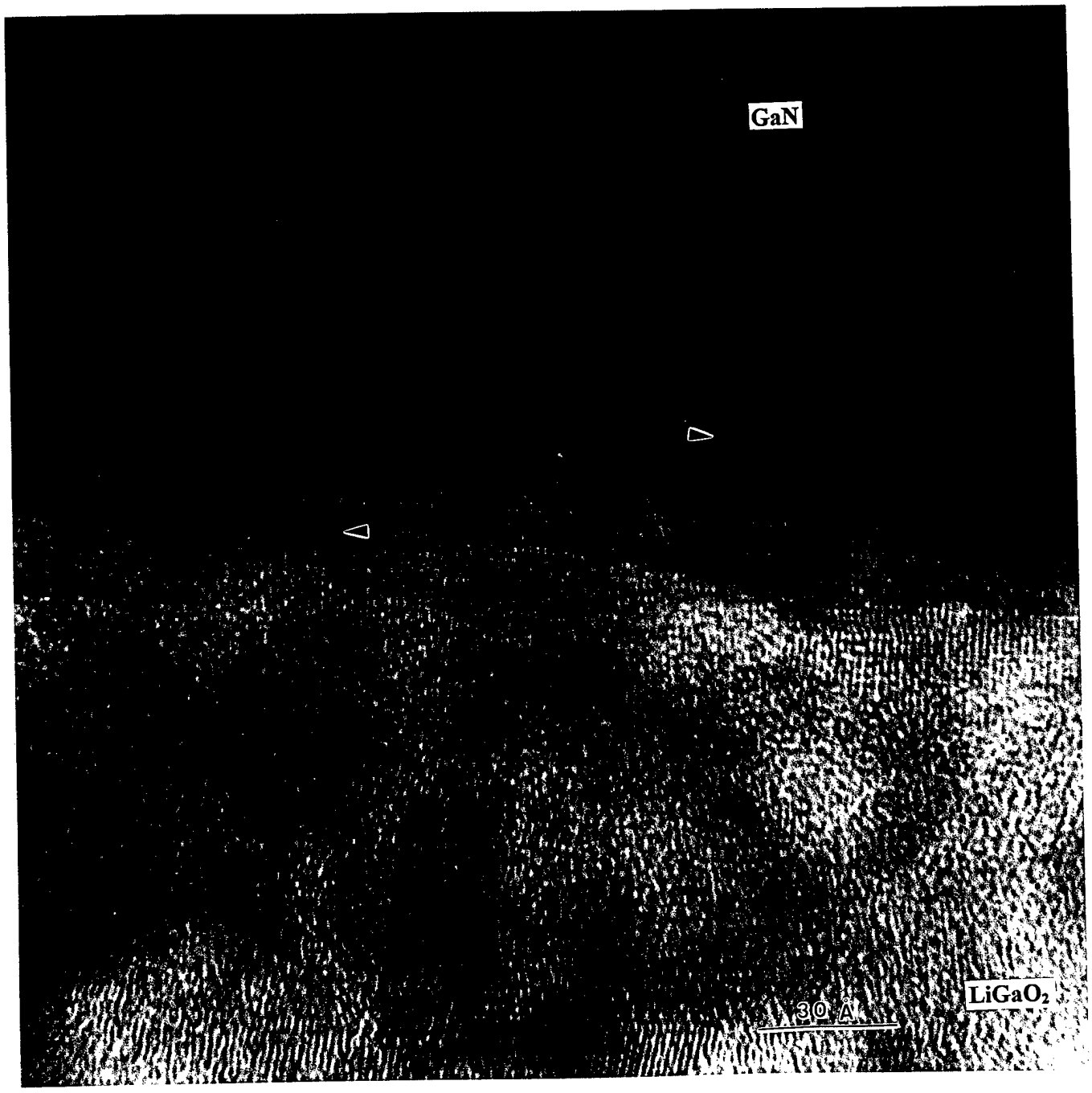

Fig. IV.6.

References:

1. H. Z. Xiao, N-E. Lee, R. C. Powell, Z. Ma, L. J. Chou, L. H. Allen, J. E. Greene and A. Rockett, J. Appl. Phys., **76** (12), 8195 (1994)
2. D. J. Smith, D. Chandraskhar, B. Sverdlov, A. Botchkarev, A. Salvador and H. Morkoc, Appl. Phys. Lett., **67** (13), 1830 (1995)
3. F. R. Chien, X. J. Ning, S. Stemmer, P. Pirouz, M. D. Bremser and R. F. Davis, Appl. Phys. Lett., **68** (19), 2678 (1996)
4. F.A. Ponce, B. S. Krusor, J. S. Major, Jr., W. E. Plano and D. F. Welch, Appl. Phys. Lett., **67**(3), 410 (1995)

(V) MOCVD Growth of GaN Thin Films (Tim Anderson, Olga Kryliouk, Todd Dann)

A major limitation to the development of GaN-based optoelectronic devices is the lack of a suitable substrate material that is lattice-matched and both thermally and chemically compatible with GaN. Furthermore, the high growth temperature typically used for MOCVD growth of GaN on sapphire severely limits the extent of In incorporation and thus the range of accessible wavelengths. The goal of this research has been to develop a lower temperature growth process (<850°C) to achieve deposition of AlGaInN over the full composition range. Specifically, we have been investigating new oxide-based substrates, including $LiGaO_2$, as a promising candidates.

Recent efforts have focused on the structural quality of GaN grown on $LiGaO_2$. Cross-sectional transmission electron microscope (XTEM) analysis shows a superior structural quality of the GaN film grown on (001) $LiGaO_2$, as detailed elsewhere in this report. Figs. IV.3a-c, IV.4a-d, and IV.5 show cross-sectional TEM micrographs of a sample grown at 850°C, V/III ratio of 3300, and a reactor pressure of 130 Torr. The GaN was deposited in a low-pressure, horizontal, cold-wall MOCVD reactor using triethylgallium (TEGa) and ammonia (NH_3) precursors and N_2 as a carrier gas. The threading dislocation density ranged from $10^9/cm^2$ at the interface to $10^7/cm^2$ at ~0.3 μm away from the interface. The upper portion of the GaN film exhibited an extremely low extended defect density, approaching that reported for homoepitaxy of GaN. The dislocation density, however is higher in the 50-nm-thick region near the film substrate interface. According to XTEM results there is an amorphous or nanocrystalline inter-layer between the film and substrate. The present results suggest that either the chemical-mechanical polishing of the $LiGaO_2$ surface did not effectively remove the slicing damage or the near surface microstructure/composition was altered during the initial stages of growth. This latter mechanism is perhaps related to Li diffusion into the GaN, or surface reaction with the gas phase reactants, or stress induced due to the slight mismatch between $LiGaO_2$ and the harder GaN film.

We have had some difficulty in assessing the film quality precisely using HRXRD as the film thickness (0.5 μm) is smaller than the X-ray penetration depth (3 to 5 μm). As a result the signal intensity originating from the substrate dominates the spectrum. We plan to grow thick (~5 μm) GaN films for further characterization.

Evidence exists that there is significant diffusion of Li into the GaN, even at this relatively low growth temperature. We are currently investigating the extent of interdiffusion by characterizing films by SNMS, SIMS, AES and XTEM as a function of annealing conditions.

During this quarter we have initiated studies on the $LiGaO_2$ substrate preparation procedure and the influence of $LiGaO_2$ nitridation on the properties of GaN films grown by MOCVD. Before receiving the $LiGaO_2$ (001) substrates, they were oriented by X-ray diffraction, sliced into wafers and polished. The last polishing step is a colloidal silica chemo-mechanical polishing to epi-grade quality.

As a first experiment, we studied the effect of surface nitridation as a function of temperature prior to film growth in terms of surface morphology and surface chemical composition. The surface morphology of the substrates and films was determined by Atomic Force Microscopy (AFM), while the composition was analyzed by Auger Electron Spectroscopy (AES).

In these experiments, as-received polished $LiGaO_2$ substrates were first cleaned with acetone and methanol solvents. The substrates were then inserted in the reactor and exposed a N_2 flow at a temperature between 650 and 900°C for 10 min. This was followed by a nitridation step using NH_3.

The surface topography of the treated $LiGaO_2$ (001) substrates as determined by AFM is displayed in Figs. V.1a-d and V.2a-d and the RMS roughness, R_g, determined from the measurements is summarized in Table V.1.

Table V.1. RMS surface roughness as a function of NH_3 exposure temperature.

Treatment	**RMS (R_g), nm**
As-received	3.40
650°C(NH_3)	0.58
800°C(NH_3)	0.12
900°C(NH_3)	0.10

The surface roughness is observed to decrease significantly as compared with the as-received substrates upon exposure to NH_3 at elevated temperature. Surface flatness is further improved with increasing NH_3 exposure temperature. Figs. V.3a-d show the results of an AES investigation of the $LiGaO_2$ (001) surface treated in NH_3 at 650, 800, and 900°C. AES analysis on the as-received $LiGaO_2$ sample surface indicated the presence of oxygen and carbon (disappeared after 30 s of Ar^+ sputtering). After NH_3 pretreatment, N was detected on the surface, and the Ga/N ratio decreased from 5.14 to 4.05 as the temperature increased from 800 to 900°C (Table V.2). The Ga/O ratio also increased from 0.44 on the as-received sample surface to 0.69 on the surface pretreated at 900°C.

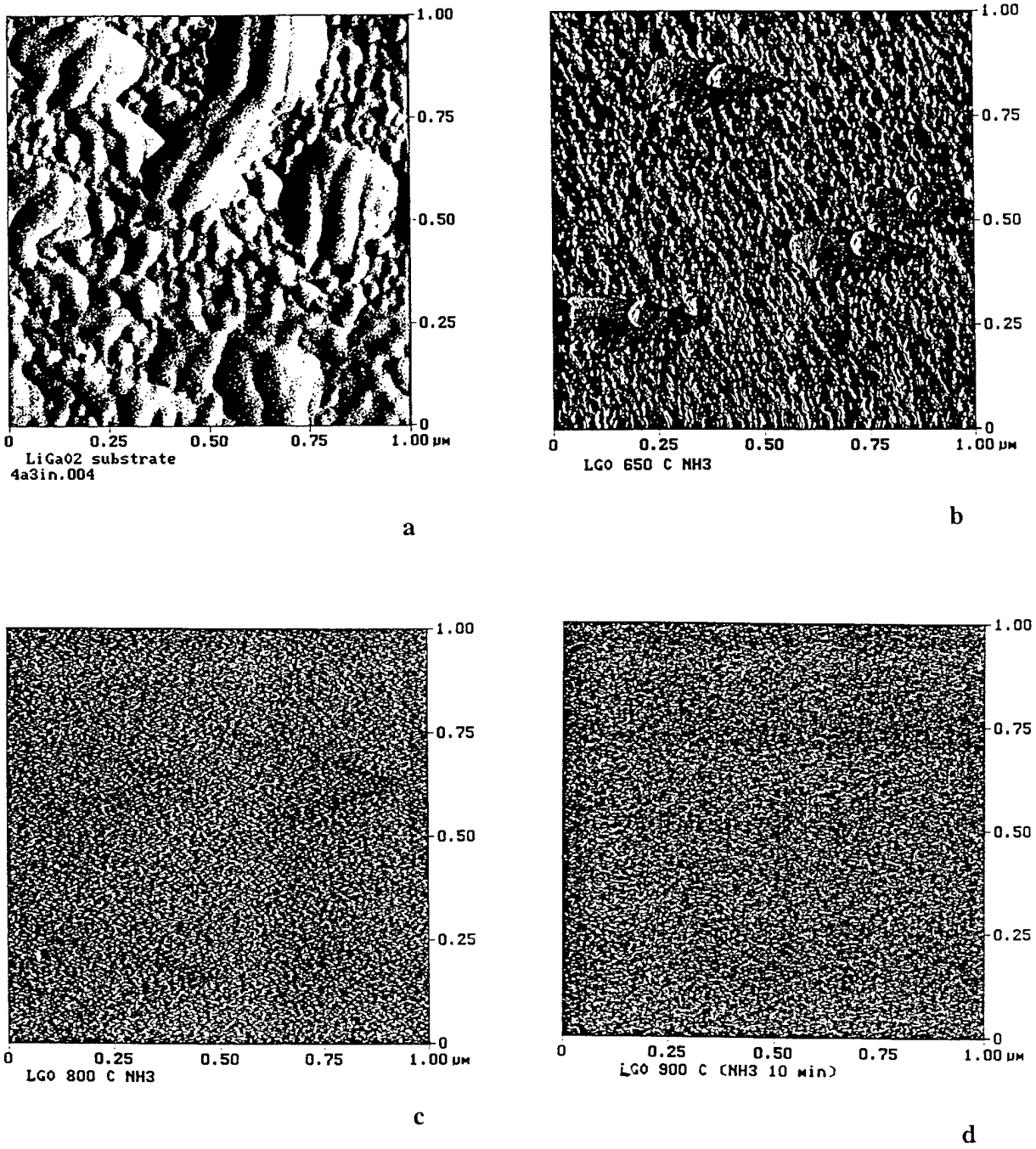

Fig. V.1a-d. AFM images of $LiGaO_2(001)$ surfaces:

a) as received

b) after 10 min NH_3 treatment, T = 650 °C

c) after 10 min NH_3 treatment, T = 800 °C

d) after 10 min NH_3 treatment, T = 900 °C

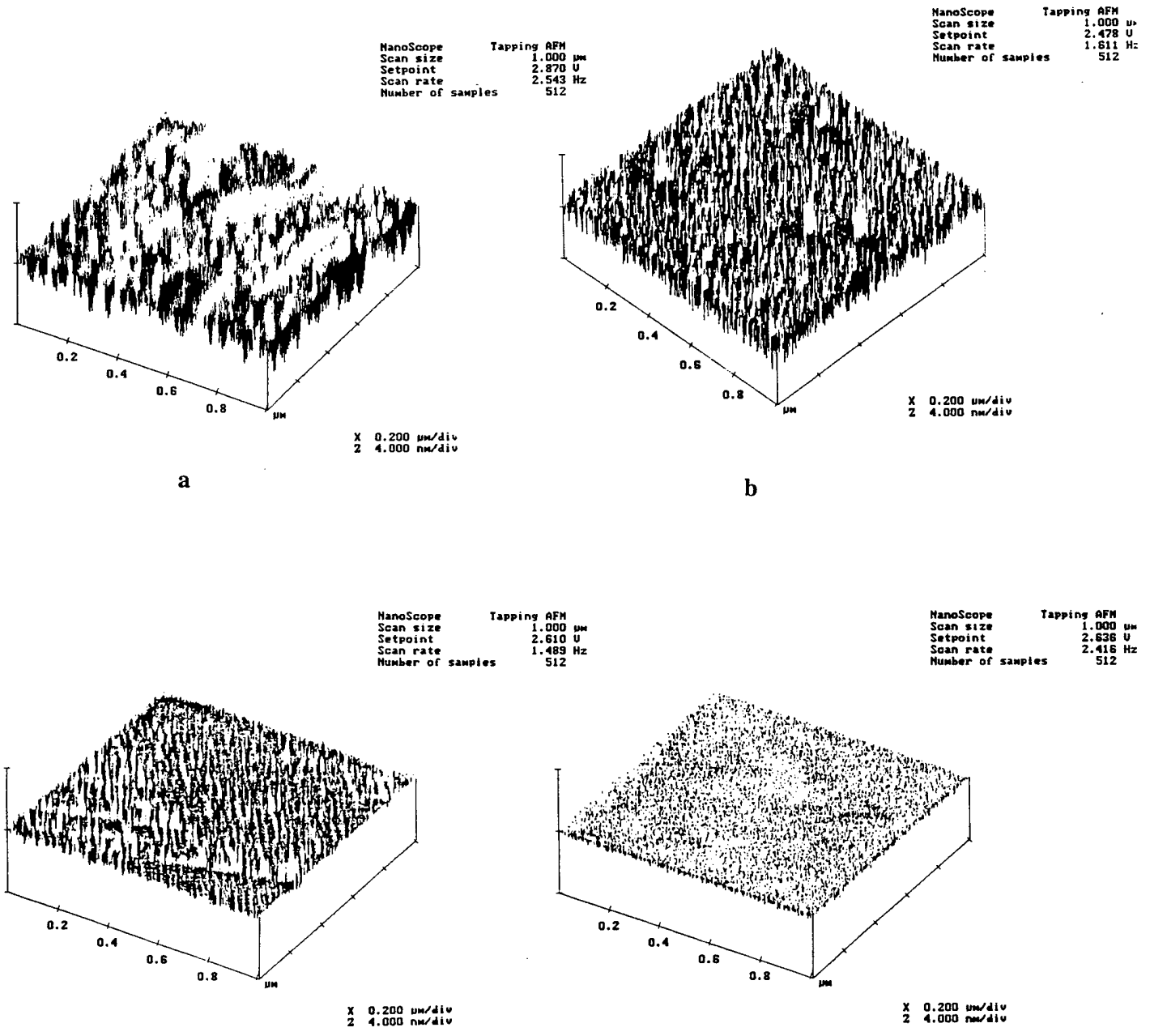

Fig. V.2a-d. 3-Dimentional view of $LiGaO_2(001)$ surfaces:

a) as received

b) after 10 min NH_3 treatment, T = 650 °C

c) after 10 min NH_3 treatment, T = 800 °C

d) after 10 min NH_3 treatment, T = 900 °C

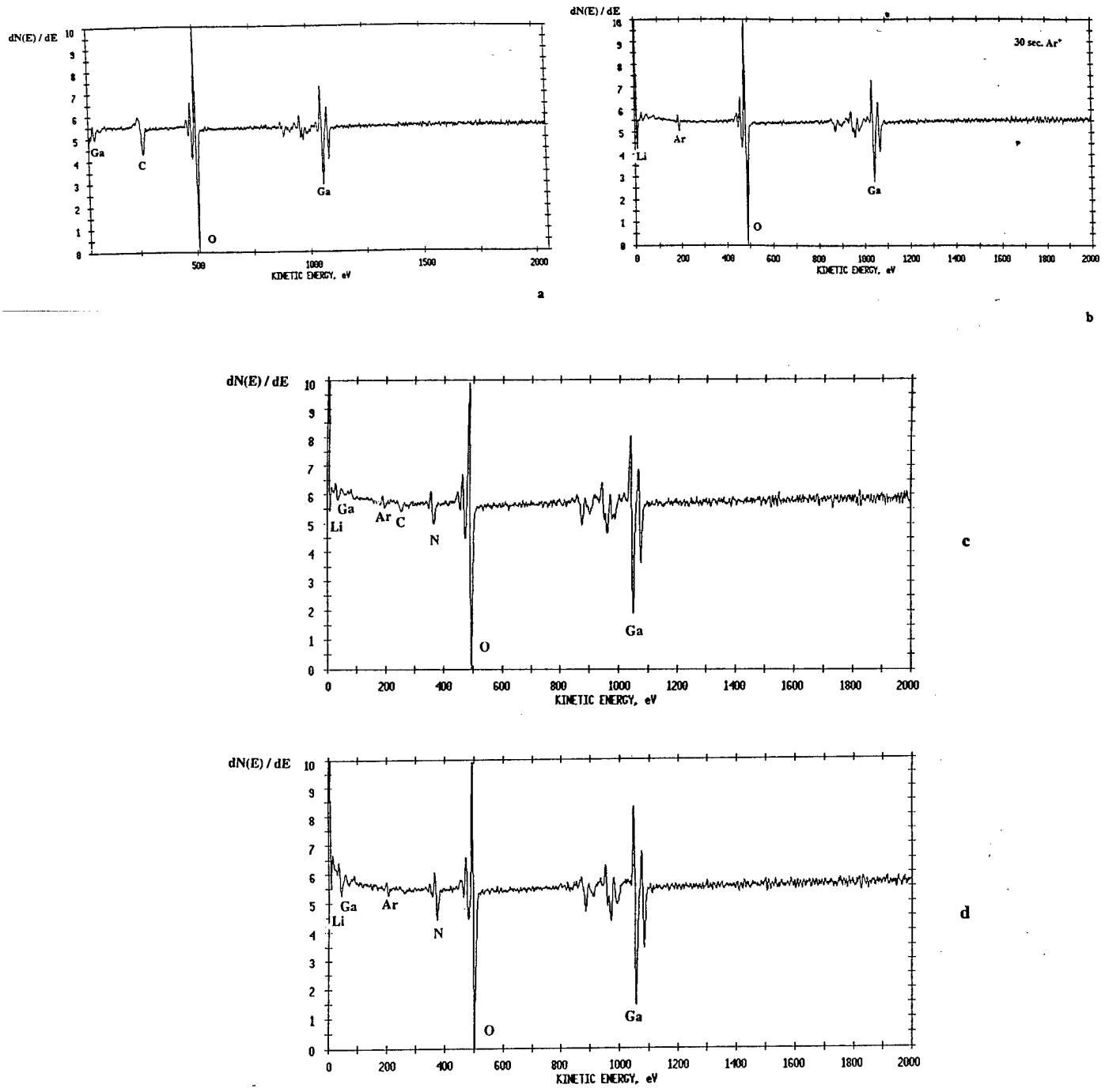

Fig. V.3a-d. AES Spectra of $LiGaO_2$ (001) surfaces: a) as received, b) after 10 min. NH_3 treatment, T = 650°C, c) after 10 min NH_3 treatment, T = 800°C, d) after 10 min NH_3 treatment, T = 900°C.

Table V.2. AES analysis of $LiGaO_2$ untreated and treated substrates

Treatment	Atomic Ratio of Ga/O	Atomic Ratio of Ga/N	Carbon	N Intensity
As-received	0.51 0.44	-	present -	-
650°C(NH_3)	0.47 0.55	-	present -	7.8
800°C(NH_3)	0.64	5.14	-	18.2
900°C(NH_3)	0.69	4.05	-	26.59

A simple thermodynamic analysis of nitridation of binary oxides (Ga_2O_3 and Li_2O) indicates preferential formation of GaN compound as compared to Li_3N. However, mixed oxides or more complex nitride could also have been formed.

The results on analysis of the surface morphology by AFM of GaN films as a function of the surface pretreatment is shown in Figs. V.4a-c and V.5a-c and Table V.3.

Table V.3. Surface roughness of GaN Films as a function of pretreatment

Treatment	Growth Temperature (° C)	RMS (R_g) (nm)
650°C(NH_3)	850	0.987
800°C(NH_3)	800	0.080
900°C(NH_3)	900	0.032

Growth of GaN on substrates pretreated in NH_3 at 650°C showed a very rough surface, with apparent 3-d growth mode. The surface morphology of GaN film grown on $LiGaO_2$(001) pretreated NH_3 at 800 and 900°C, however, were very smooth, consistent with a 2-d growth mode.

Figs. V.6a-b, V.7a-b and V.8a-b shows AES spectra, depth profiles and surface scans for GaN films grown at 850°C on $LiGaO_2$ (001) pretreated with NH_3 (10 min) and substrates with no pretreatment (NH_3 and TEGa flows simultaneously initiated). On both samples the surface was contaminated with oxygen from a native oxide. The oxygen appears only in the top 50 Å of the surface of the sample after NH_3 treatment. From these data, the estimated transition layer thickness observed when using the pretreated substrate (~400 Å) is twice as thick as observed when using no surface pretreatment.

The essential role of the nitridation is thought to be supplying nucleation centers of GaN having the same orientation as the substrate and the promotion of 2nd GaN film growth through the decrease in interfacial free energy between the film and substrate. It could also play a role in Li diffusion from the substrate into the GaN film, and this is under further investigation.

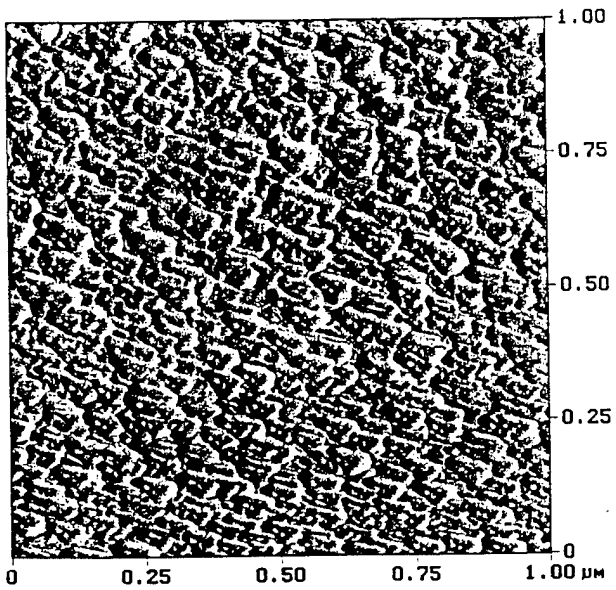

a

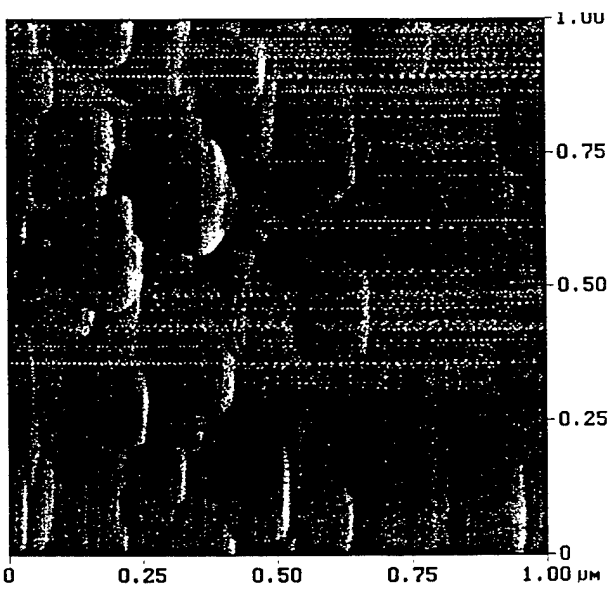

b

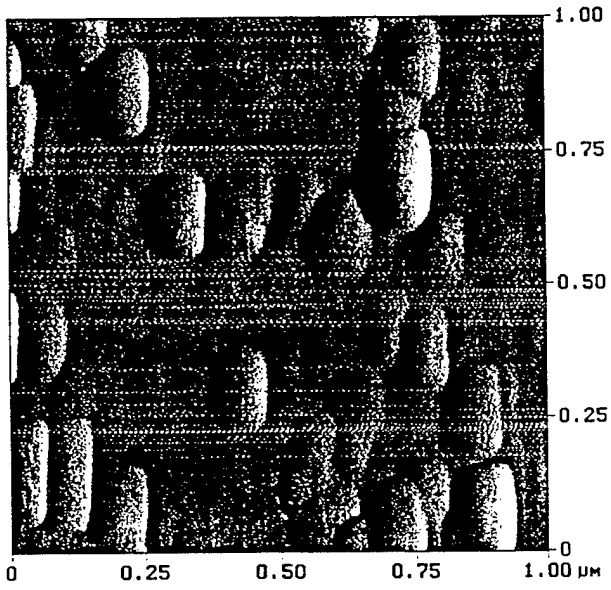

c

Fig. V.4a-c. AFM images of GaN films (film thickness = 85 Å) grown on $LiGaO_2(001)$:

a) after 10 min NH_3 treatment, T = 650 °C

b) after 10 min NH_3 treatment , T = 800 °C

c) after 10 min NH_3 treatment, T = 900 °C

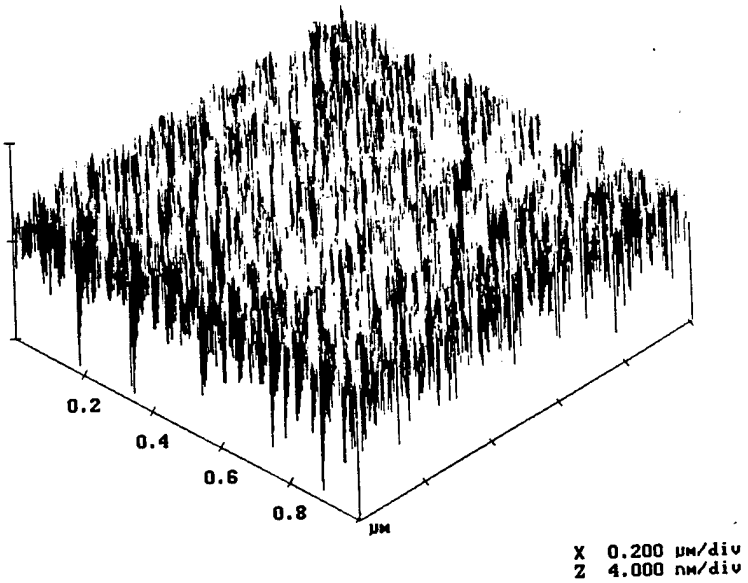

a

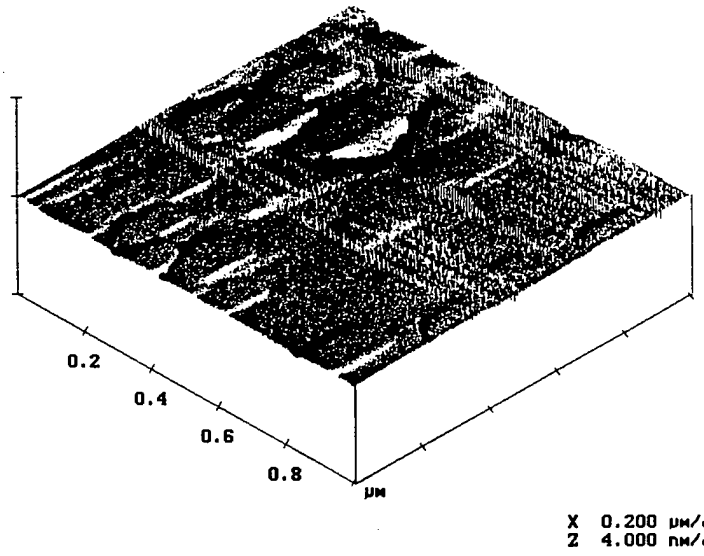

b

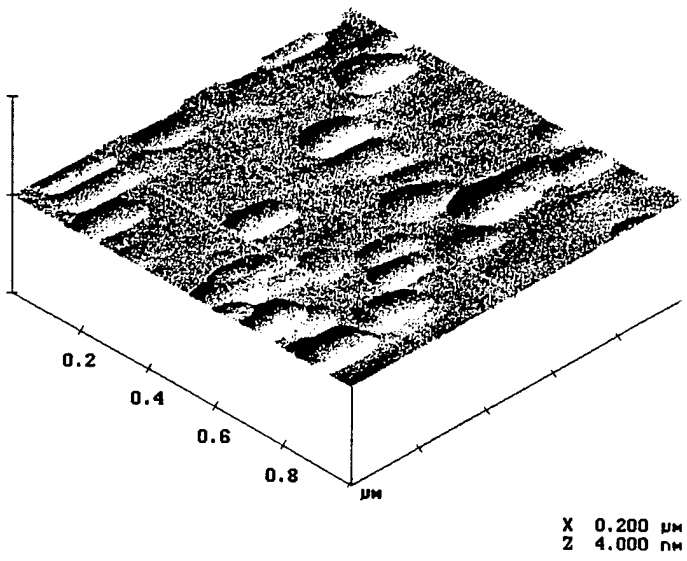

c

Fig. V.5a-d. 3-dimentional view of GaN films (film thickness = 85 Å) grown on $LiGaO_2(001)$:

a) after 10 min NH_3 treatment, T = 650 °C

b) after 10 min NH_3 treatment, T = 800 °C

c) after 10 min NH_3 treatment, T = 900 °C

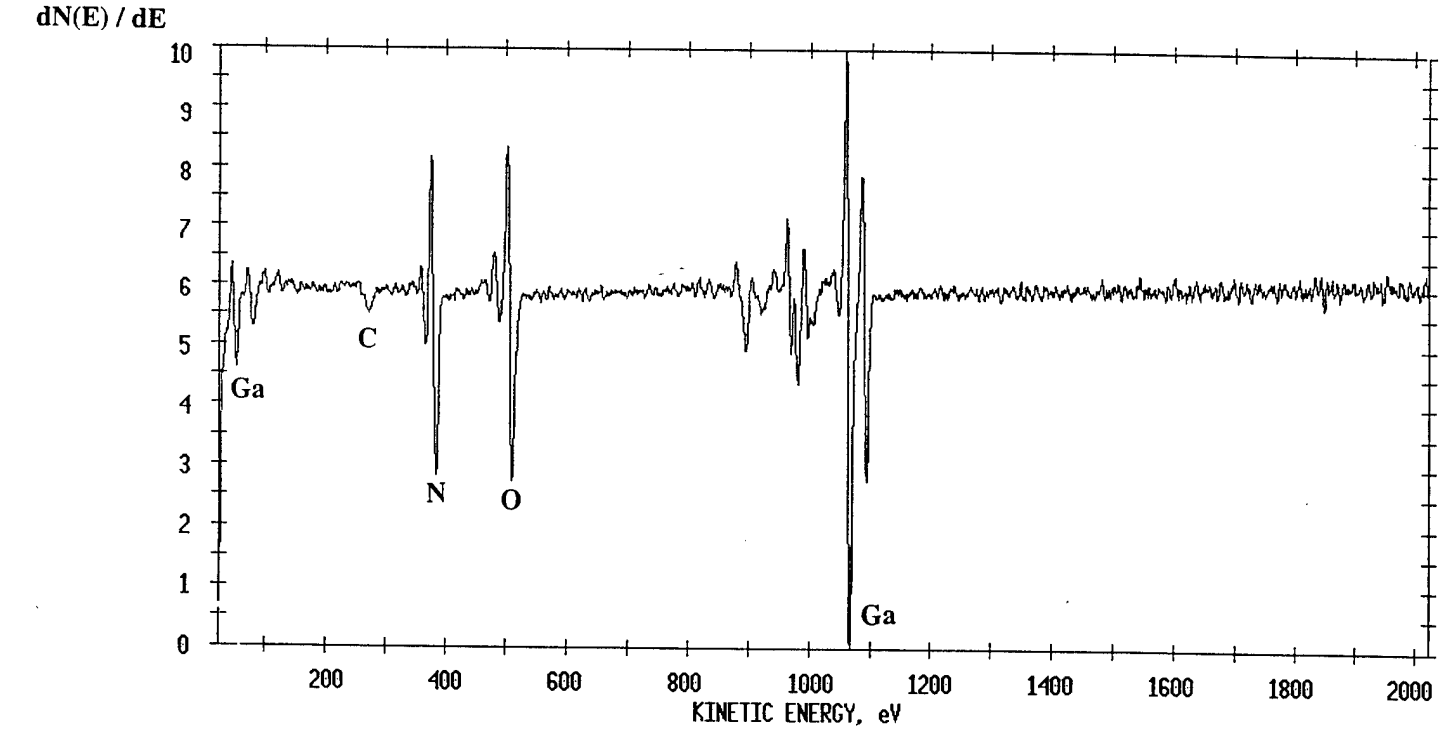

a

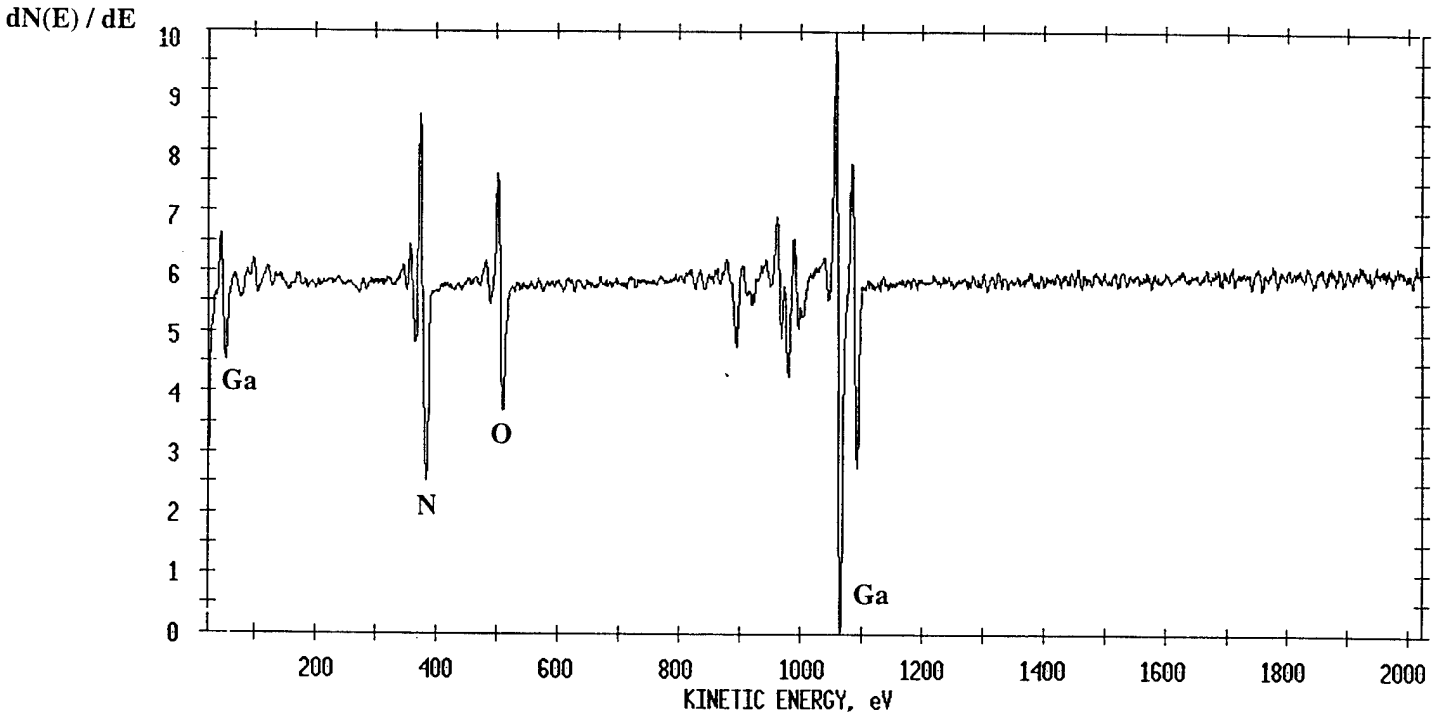

b

Fig. V.6a-b. AES spectra of GaN films grown on $LiGaO_2$ (001)
Tg = 850°C, V/III ratio = 3300, Growth pressure = 110 Torr:
a) after $LiGaO_2$ substrate nitridation 10 min NH_3, T = 850°C
b) non-nitrided $LiGaO_2$ surface

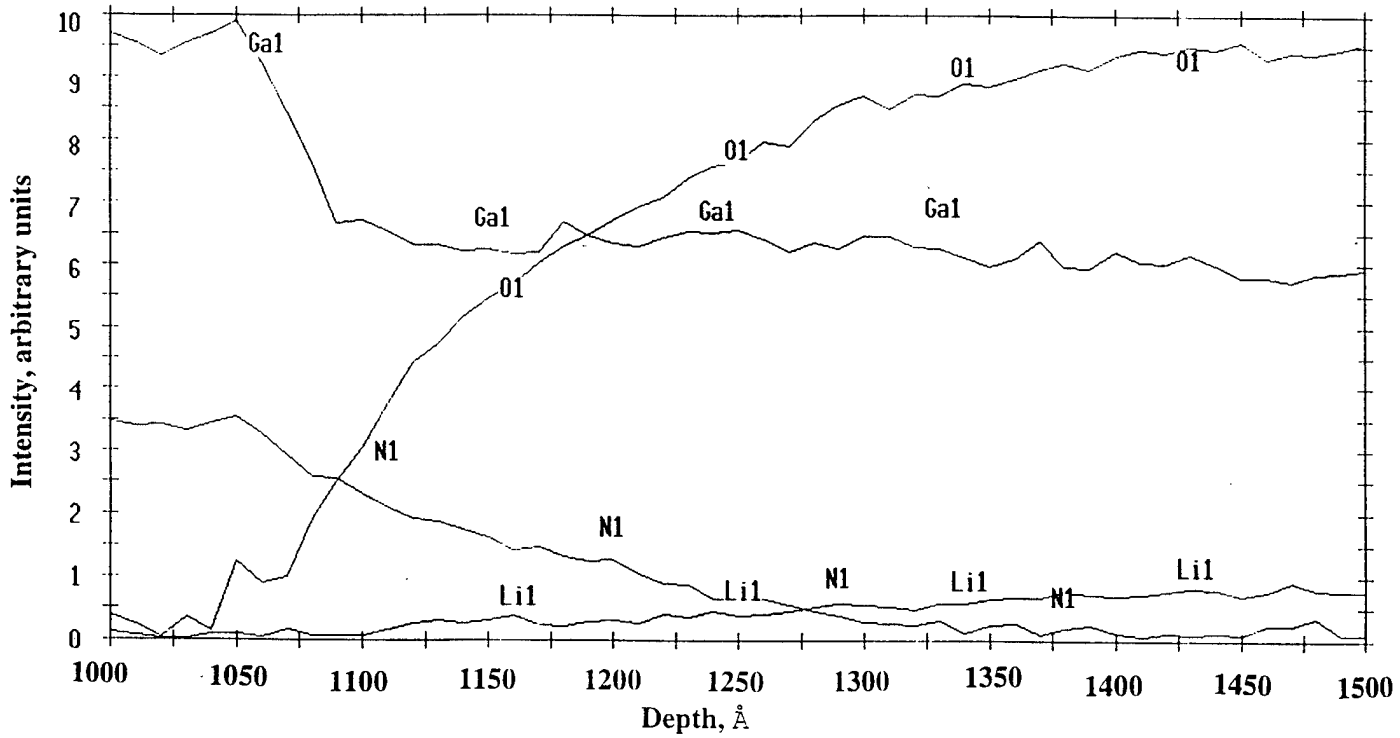

a

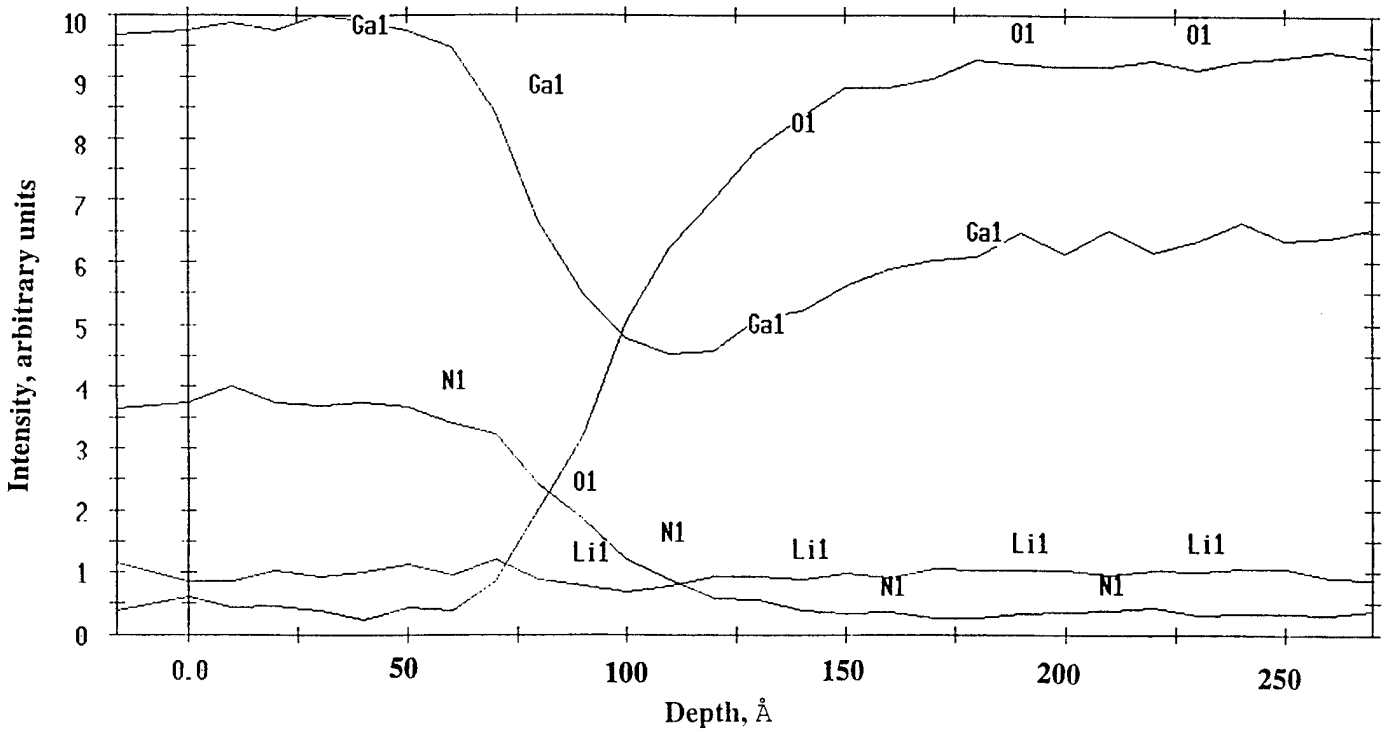

b

Fig. V.7a-b. AES depth profiles of GaN films grown on LiGaO2 (001)

Tg = 850 C, V/III ratio = 3300, Growth pressure = 110 Torr:

a) after $LiGaO_2$ substrate nitridation 10 min NH_3, T = 850 °C

b) non-nitrided $LiGaO_2$ surface

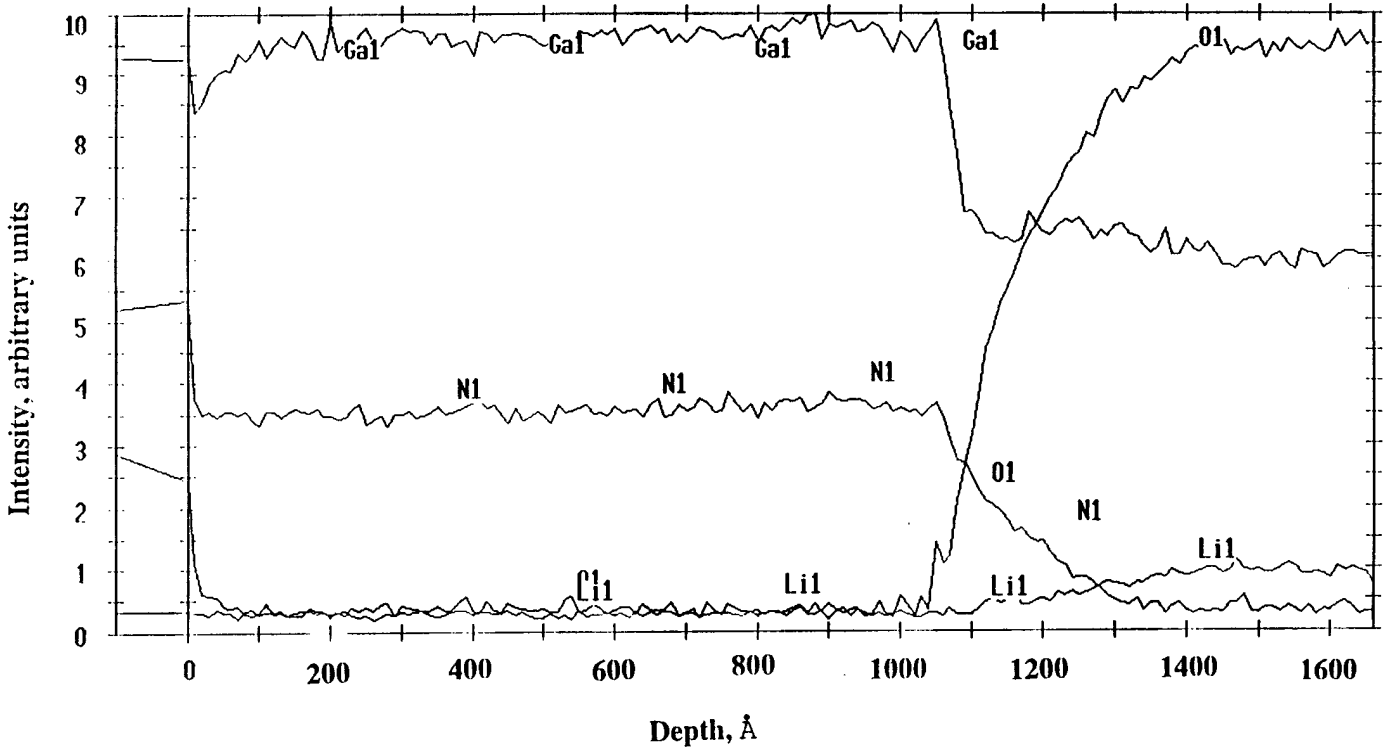

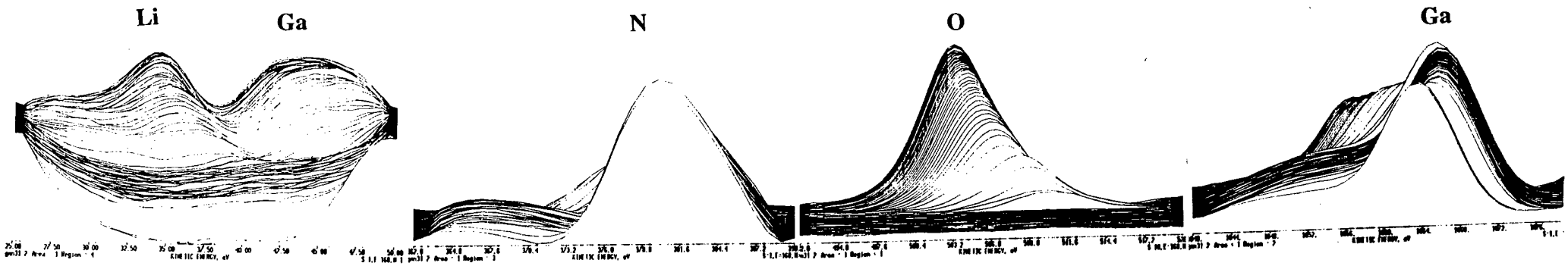

Fig. V.8a. AES depth profile of GaN film grown on $LiGaO_2$ (001)
Tg = 850°C, V/III ratio = 3300, Growth pressure = 110 Torr:
a) after $LiGaO_2$ substrate nitridation 10 min NH_3, T = 850°

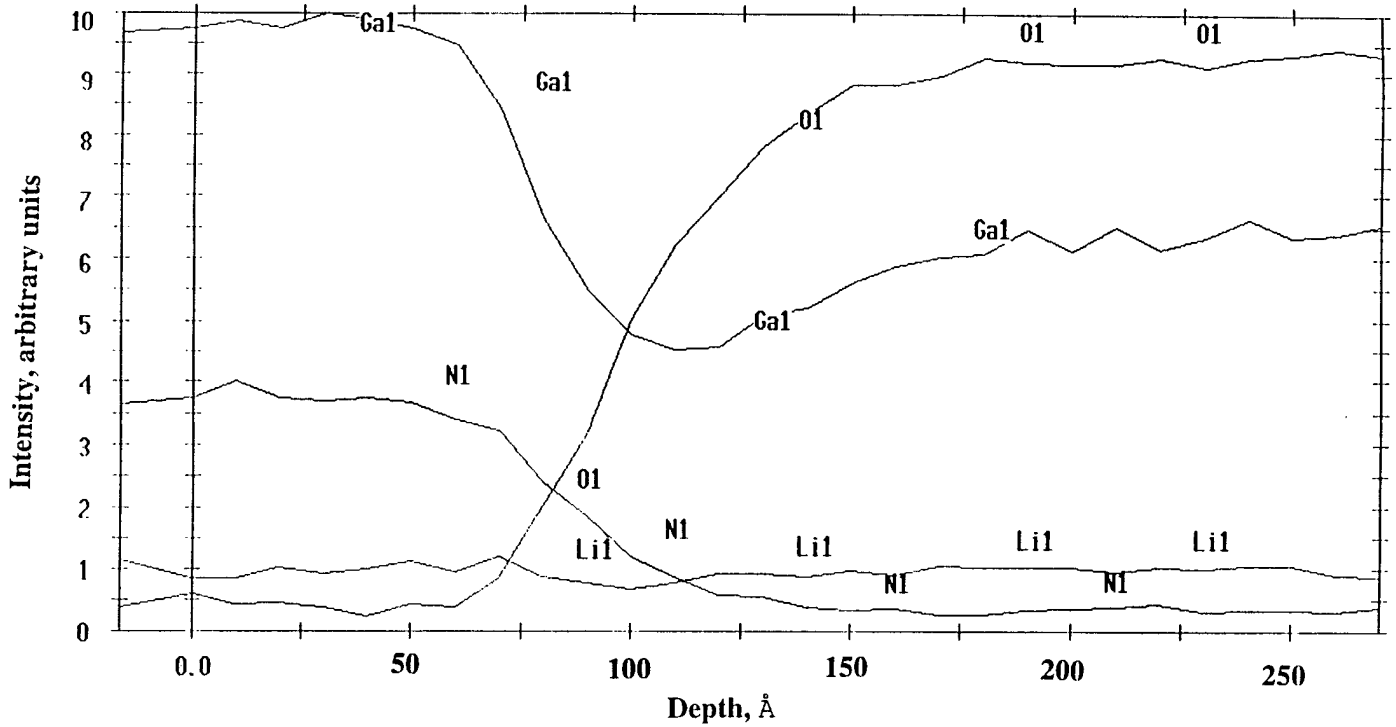

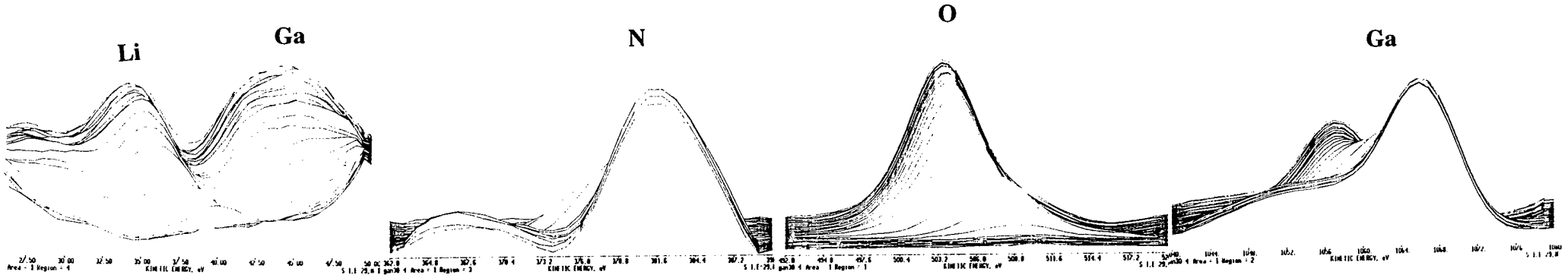

Fig. V.8b. AES depth profile of GaN film grown on $LiGaO_2$ (001) Tg = 850°C, V/III ratio = 3300, Growth pressure = 110 Torr: b) non-nitrided $LiGaO_2$ surface

(VI) Diode Laser Materials (Peter Zory)

VI.a. CdZnSe Quantum Well (QW) Diode Laser Material

Work is continuing to establish the importance of Coulomb enhancement and other many-body effects in predicting the performance of wide bandgap lasers in general, and CdZnSe QW lasers in particular. The dependence of lasing wavelength on laser length for CdZnSe single quantum well, buried ridgeguide lasers provided by Michael Haase of 3M has been measured. The "slope" of the data is in good agreement with the slope calculated from a free carrier quantum well laser model modified to include wavelength shifts due to carrier scattering (CS), bandgap renormalization (BGR) and Coulomb enhancement (CE). However, it is interesting to note that good agreement could also have been obtained if BGR and CE had been ignored and the carrier scattering time used had been decreased by a factor of 2. Additional measurements of other parameters such as laser threshold and spontaneous emission spectra are underway in order to remove this ambiguity. Our collaboration on the theoretical aspects of the many-body problem with Paul Rees, now located at the University of Wales, Bangor, is continuing.

VI.b. InGaN QE LED Material

We are continuing work on the liquid contact luminescence (LCL) technique for evaluating the light emitting capabilities of p-GaN/InGaN/n-GaN LED material. One problem in using this technique is the generation of hydrogen bubbles in the hole injection process. We have developed a new electrolyte which provides hole injection without bubble generation and are in the process of determining how well it works with nitride materials. The LCL technique was discussed and demonstrated at the workshop on nitride LED materials held in conjnction with the CLEO in June in Anaheim, CA (workshop chaired by Jo Major of SDL).

Short Course:

- "Visible Semiconductor Lasers," taught by D. Bour and P. Zory at the Conference on Electro-optics and Lasers (CLEO), Anaheim, CA, June 1996.

Publications:

- "Process Development for III-V Nitrides," S.J. Pearton, C.R. Abernathy, F. Ren, R.J. Shul, S.P. Kilcoyne, M.H. Crawford, J.C. Zolper, R.G. Wilson, R.N. Schwartz and J.M. Zavada, Mat. Sci. Eng. B 38, 138 (1996).
- "Minority Carrier Enhanced Reaction of Hydrogen-Passivated Mg in GaN," S.J. Pearton, J.W. Lee and C. Yuan, Appl. Phys. Lett. 68, 2690 (1996).
- "Ion Implantation and Rapid Thermal Processing of III-V Nitrides," J.C. Zolper, M.H. Crawford, S.J. Pearton, C.R. Abernathy, C.B. Vartuli, C. Yuan and R.A. Stall, J. Electron. Mater. 25, 839 (1996).
- "Sputtered AlN Encapsulant for High Temperature Annealing of GaN," J.C. Zolper, D.J. Rieger, A.G. Baca, S.J. Pearton, J.W. Lee and R.A. Stall, Appl. Phys. Lett. 69, 538 (1996).
- "Unintentional Hydrogenation of GaN and Related Alloys During Processing," S.J. Pearton, C.R. Abernathy, C.B. Vartuli, J.W. Lee, J.D. MacKenzie, R.G. Wilson, R.J. Shul, F. Ren and J.M. Zavada, J. Vac. Sci. Technol. A 14, 831 (1996).
- "Patterning of AlN, InN and GaN in KOH-based Solutions," J.R. Mileham, S.J. Pearton, C.R. Abernathy, J.D. MacKenzie, R.J. Shul and S. Kilcoyne, J. Vac. Sci. Technol. A 14, 836 (1996).
- "High Density Plasma Etching of III-V Nitrides," C.B. Vartuli, S.J. Pearton, C.R. Abernathy, R.J. Shul, A.J. Howard and J.E. Parmeter, J. Vac. Sci. Technol. A 14, 1011 (1996).
- "Magnetron RIE of Group III-Nitride Ternary Alloys," G.F. McLane, T. Monahan, D.W. Eckart, S.J. Pearton and C.R. Abernathy, J. Vac. Sci. Technol. A 14, 1046 (1996).
- "Thermal Stability of W Ohmic Contacts to n-type GaN," M. Cole, T. Monahan, F. Ren, R. Stall, S.J. Pearton, Y. Li and Y. Lu, J. Appl. Phys. 80, 278 (1996).
- "Effect of BCl_3 Dry Etching and InAlN Surface Properties." F. Ren, J. Lothian, Y.K. Chen, S.M. Donovan, C.B. Vartuli, C.R. Abernathy, J.W. Lee and S.J. Pearton, J. Electrochem. Soc. 143, L217 (1996).
- "Microstructural Stability of Ohmic Contacts to InGaN," A. Durbha, S.J. Pearton, C.R. Abernathy, J.W. Lee, P.H. Holloway and F. Ren, J. Vac. Sci. Technol. B 14, 2582 (1996).
- "Comparison of Dry Etch Techniques for GaN," R.J. Shul, G. McClellan, S.J. Pearton, C.R. Abernathy, C. Constantine and C. Barratt, Electron. Lett. 32, 1408 (1996).
- "Inductively Coupled Plasma Etching of GaN," R.J. Shul, D.J. Rieger, S.J. Pearton, C. Constantine and R. Karlicek, Appl. Phys. Lett. 69, 1119 (1996).
- "Formation of Ohmic Contacts to p-ZnTe," J.T. Trexler, J.J. Fijol, L.C. Calhoun, R.M. Park, and P.H. Holloway, J. Electron. Matl. **25**, 1474 (1996).
- "Interfacial Reactions Between Metal Thin Films and p-GaN," J.T. Trexler, S.J. Miller, P.H. Holloway, and M.A. Khan, Mat. Res. Soc. Symp. Proc. **395**, 819 (1996).

Presentations:

- A. Weinstein, T.M. Ritter, D. Strachan, M. Li, H. Luo, M. Tamargo and R.M. Park, Competion of deep and shallow impurities in wide gap II-VI's under pressure," 7th International Conference on High Pressure Semiconductor Physics, Schwabish-Gemund, Germany, July 28-31, 1996. (paper to be published in Physica Status Solidi).
- L.C. Calhoun, M.H. Jeon, M.H. Ludwig and R.M. Park, "Reduction of the stacking fault concentration in ZnSe epilayers through surface stoichiometry control," Workshop on the future direction of II-VI semiconductors materials and devices, SUNY Buffalo, NY, Aug. 6-17, 1996.

Post Doctoral Associates:

Jing Hong Li with Dr. Jones
Olga Kryliouk with Dr. Anderson

Graduate Students Supported:

Bruce Liu with Dr. Park
George Kim with Dr. Park
Brent Gila with Dr. Park
Jin Hong with Dr. Pearton
K.N. Lee with Dr. Abernathy
Jeff Trexler with Dr. Holloway
Joe Thomes with Dr. Holloway
Todd Dann with Dr. Anderson
Jeff Hsu with Dr. Zory
Jason O with Dr. Zory